shaking. Binding experiments were carried out as described previously.[14] [^{125}I]DMFV ([^{125}I]6-iodo-4'-dimethylaminoflavone) with 81.4 TBq/mmol specific activity and greater than 95% radiochemical purity was prepared using the standard iododestannylation reaction.[14] A mixture containing 50 μL of test compounds (0.2 pM–400 μM in 10% EtOH), 50 μL of 0.02 nM [^{125}I]DMFV, 50 μL of Aβ(1-42) aggregates and 850 μL of 10% EtOH was incubated at room temperature for 3 h. The mixture was then filtered through Whatman GF/B filters using a Brandel M-24 cell harvester, and the radioactivity on the filters containing the bound ^{125}I ligand was measured in a gamma counter (Aloka, ARC-380). Values for the half-maximal inhibitory concentration (IC_{50}) were determined from displacement curves of three independent experiments using GraphPad Prism 4.0, and those for the inhibition constant (K_i) were calculated using the Cheng-Prusoff equation:[18] $K_i = IC_{50}/(1 + [L]/K_d)$, where [L] is the concentration of [^{125}I]DMFV used in the assay, and K_d is the dissociation constant of DMFV (12.3 nM).[14]

2.4. Staining of amyloid plaques in transgenic mouse brain sections

Animal studies were conducted in accordance with institutional guidelines and approved by the Kyoto University Animal Care Committee. Tg2576 transgenic mice (female, 20-month-old) were used as an Alzheimer's model. While under isoflurane anesthesia, the mice were sacrificed by decapitation, and the brains were immediately removed and frozen in powdered dry ice. The frozen blocks were sliced into serial sections 10 μm thick using a cryostat (Leica Instruments, CM1900). Each slide was incubated with a 50% ethanol solution (100 μM) of compound **8a**, **8b**, or **8c**, which have the characteristics to emit fluorescence. The sections were washed in 50% ethanol for 3 min two times, and examined using a microscope (Nikon, Eclipse 80i) equipped with a B-2A filter set (excitation, 450–490 nm; dichronic mirror, 505 nm; longpass filter, 520 nm). Thereafter, the serial sections were also immunostained with DAB as a chromogen using monoclonal antibodies against β-amyloid (Amyloid β-Protein Immunohistostain kit, WAKO).

2.5. In vivo biodistribution in normal mice

A saline solution (100 μL) containing ethanol (5 μL) of radiolabeled agents (18.5 kBq) was injected directly into a tail vein of ddY mice (5-week-old, 22–25 g). While under isoflurane anesthesia, the mice were sacrificed at various time points postinjection. The organs of interest were removed and weighed, and radioactivity was measured with an automatic gamma counter (Packard Cobra Auto-Gamma Counter 5003).

3. Results and discussion

The target FPEG flavone derivatives were prepared as shown in Scheme 1. The most common method of synthesizing flavones is known as the Baker-Venkataraman transformation.[19] In this process, a hydroxyacetophenone is first converted into a benzoyl ester **1**, and this species is then treated with a base, forming a 1,3-diketone **2**. Treatment of this diketone with acid leads to generation of the desired flavone **3**. In the route for the synthesis of dimethylamino derivatives, the free amino derivative **4** was readily prepared from **3** by reduction with $SnCl_2$. Compound **5** was converted to **6** by demethylation with BBr_3 in CH_2Cl_2. To prepare compounds with 1-3 ethoxy groups as the PEG linkage, commercially available chlorides were coupled with the OH group of **6** to obtain **7(a–c)**, respectively. The fluorinated flavones, **8(a–c)**, were successfully obtained by reacting **7(a–c)** with DAST in DME or ethylene glycol dimethyl ether. In the route for the synthesis of monomethylated derivatives and the primary amino derivatives, the demethylation of **3** with BBr_3 and the introduction of 1-3 ethoxy groups into **9** gave **10(a–c)**. To prepare

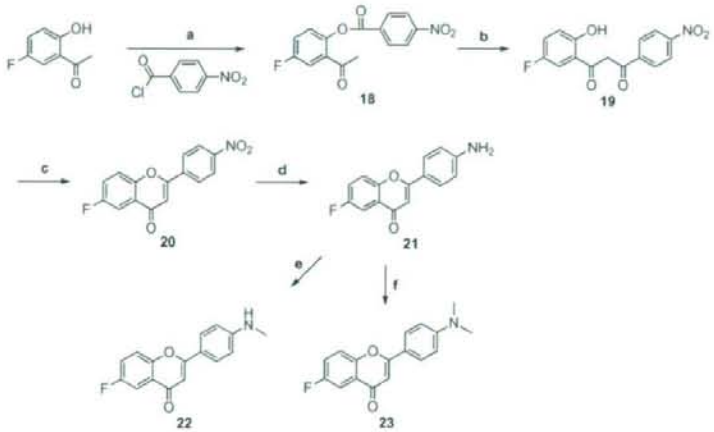

Scheme 2. Reagents: (a) pyridine; (b) KOH, pyridine; (c) H_2SO_4, AcOH; (d) EtOH, $SnCl_2$; (e) $(CH_2O)_n$, NaOMe, $NaBH_4$; (f) $(CH_2O)_n$, $NaCNBH_3$, AcOH.

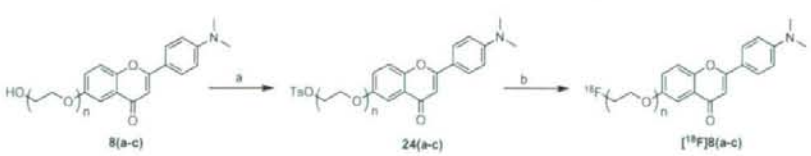

Scheme 3. Reagents: (a) tosyl chloride, pyridine; (b) K_2CO_3, [^{18}F]F^-, kryptofix[222], DMSO/acetonitrile.

Please cite this article in press as: Ono, M. et al., *Bioorg. Med. Chem.* (2009), doi:10.1016/j.bmc.2009.01.025

the FPEG flavone with one ethoxy group ($n = 1$) (**12** and **13**), the fluorination of **10a** with DAST, the reduction of **11** with $SnCl_2$ and the methylation of **12** were performed. The primary amino derivatives of FPEG flavones ($n = 2$ and 3) (**15b** and **15c**) were synthesized by the fluorination of **14b** and **14c** with DAST following the reduction of the nitro group in **10b** and **10c**. The monomethylated FPEG flavones ($n = 2$ and 3) (**17b** and **17c**) were synthesized by the methylation of **16b** and **16c** following the fluorination of **14b** and **14c** with DAST. We successfully synthesized the flavone derivatives (**21**, **22**, and **23**) with fluorine directly bound to the phenyl group according to a procedure reported previously (Scheme 2). To make the desired ^{18}F-labeled FPEG flavones, [^{18}F]**8(a–c)**, the tosylates **24(a–c)** were employed as the precursors. The free OH groups of **8(a–c)** were converted into tosylates by reacting with TsCl in the presence of pyridine to give **24(a–c)** (Scheme 3). Each of the tosylates, **24(a–c)**, was mixed with [^{18}F]fluoride/potassium carbonate and Kryptofix 222 in DMSO and heated at 160 °C for 5 min. The crude product was purified by HPLC (radiochemical purity >99%, radiochemical yield 5–13%, decay corrected). The total synthesis time was 70 min, and the specific activity was estimated to be 33.3–55.5 GBq/mmol at the end of synthesis.

Table 1
Inhibition constants (K_i, nM) of compounds for the binding of [^{125}I]DMFV to Aβ(1-42) aggregates[a]

Compound	K_i (nM)	Compound	K_i (nM)
8a	5.3 ± 0.8	**15c**	234.0 ± 60.6
8b	14.4 ± 2.5	**17b**	54.5 ± 10.3
8c	19.3 ± 4.0	**17c**	45.1 ± 5.8
12	234.3 ± 63.5	**21**	260.5 ± 43.3
13	99.0 ± 11.8	**22**	110.0 ± 47.4
15b	321.1 ± 74.4	**23**	73.9 ± 5.3

[a] Values are the mean ± standard error of the mean for 4–9 experiments.

Table 2
Biodistribution of ^{18}F-labeled flavones in normal mice[a]

Organ	2 min	10 min	30 min	60 min
*[^{18}F]**8a***				
Blood	2.80 ± 0.41	2.71 ± 0.13	2.53 ± 0.17	3.25 ± 0.31
Brain	4.17 ± 0.77	3.62 ± 0.21	1.89 ± 0.13	2.19 ± 0.18
Bone	2.02 ± 0.53	2.83 ± 0.23	4.51 ± 0.55	6.21 ± 0.84
*[^{18}F]**8b***				
Blood	2.09 ± 0.35	2.30 ± 0.07	2.50 ± 0.21	2.94 ± 0.27
Brain	3.54 ± 0.54	2.75 ± 0.21	2.00 ± 0.20	2.13 ± 0.10
Bone	1.13 ± 0.22	1.65 ± 0.10	2.42 ± 0.38	3.74 ± 0.30
*[^{18}F]**8c***				
Blood	2.35 ± 0.54	1.50 ± 0.26	1.40 ± 0.04	1.88 ± 0.08
Brain	2.89 ± 0.74	2.23 ± 0.36	1.31 ± 0.14	1.37 ± 0.11
Bone	1.53 ± 0.52	2.38 ± 0.39	4.06 ± 0.49	5.21 ± 0.98

[a] Expressed as % of injected dose per gram. Each value represents the mean ± SD for 4–5 mice at each interval.

In vitro binding experiments to evaluate the affinity of the FPEG flavones for Aβ aggregates were carried out in solutions with [^{125}I]DMFV as the ligand. The affinity of flavone derivatives for Aβ aggregates varied from 5 to 321 nM (Table 1). The flavone derivatives had affinity for Aβ(1-42) aggregates in the following order: the dimethyamino derivatives (**8a**, **8b**, **8c**, and **23**) > the monomethylamino derivatives (**13**, **17b**, **17c**, and **22**) > the primary amino derivatives (**12**, **15b**, **15c**, and **21**). The results of the binding experiments are consistent with those of previous reports.[14,20,21] The K_i values indicated that the affinity for Aβ(1-42) aggregates was affected by the substituted group at position 4′ in the flavone structure, not by the length of the PEG introduced into the flavone backbone. We selected the dimethylamino derivatives (**8a**, **8b**, and **8c**), which showed greater binding affinity than the monomethylamino derivatives and the primary amino derivatives, for additional study.

Three ^{18}F FPEG flavones ([^{18}F]**8a**, [^{18}F]**8b**, and [^{18}F]**8c**) were examined for their biodistribution in normal mice (Table 2). All three ligands displayed high uptake from the brain 2.89–4.17%ID/g, at 2 min postinjection, indicating a level sufficient for imaging. In addition, they displayed good clearance from the normal brain with 1.89, 2.00, and 1.31%ID/g at 30 min postinjection for [^{18}F]**8a**, [^{18}F]**8b**, and [^{18}F]**8c**, respectively. These values were equal to 45.3%, 56.5%, and 45.3% of the initial uptake peak for [^{18}F]**8a**, [^{18}F]**8b**, and [^{18}F]**8c**, respectively. A rapid initial uptake in normal brain coupled with a fast washout are highly desirable properties for β-amyloid-imaging probes, as they lead to a high signal to background ratio. [^{18}F]**8(a–c)** showed the bone uptake (3.74–6.21%ID/g) at 60 min postinjection, suggesting there may be in vivo defluorination. However, the free fluorine was not taken up by brain tissue; therefore, the interference from this free fluoride is expected to be relatively low for brain imaging.[22]

To confirm the affinity of FPEG chalcone derivatives for β-amyloid plaques in the brain, neuropathological fluorescent staining

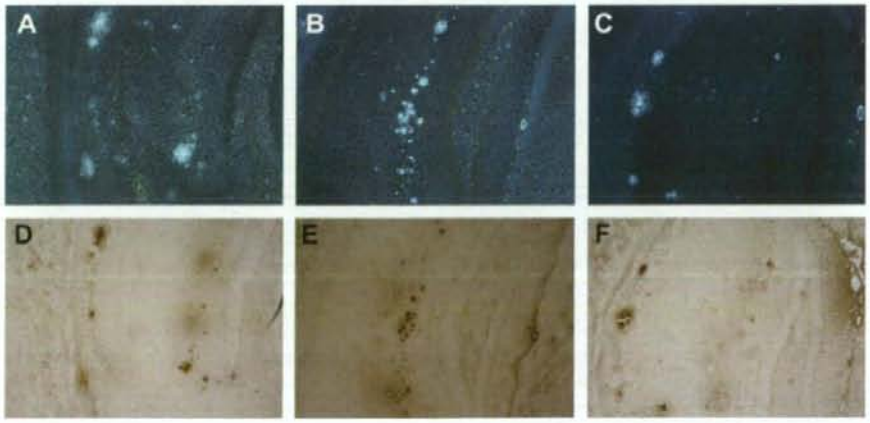

Figure 2. Neuropathological staining of flavone derivatives **8a** (A), **8b** (B), and **8c** (C) in 10-μm brain sections of Tg2576 mice. Immunohistological staining with an antibody against β-amyloid (D, E, and F) in the adjacent sections of A, B, and C, respectively.

Please cite this article in press as: Ono, M. et al., *Bioorg. Med. Chem.* (2009), doi:10.1016/j.bmc.2009.01.025

with **8a**, **8b**, and **8c** was carried out using the Alzheimer's model (Fig. 2A–C). Many fluorescence spots were observed in the brain sections of Tg2576 transgenic (female, 20-month-old) mice, while no spots were observed in the brain sections of wild-type (female, 22-month-old) mice (data not shown). The fluorescent labeling pattern was consistent with that obtained by immunohistochemical labeling with an antibody specific for Aβ (Fig. 2D–F), indicating that FPEG flavones show specific binding to β-amyloid plaques in the mouse brain.

In conclusion, we successfully designed and synthesized novel ^{18}F labeled flavones with the FPEG strategy for PET imaging of β-amyloid in the brain. The affinity of the derivatives for Aβ aggregates varied from 5 to 321 nM. When in vitro plaque labeling was carried out using sections of brain from Tg2576 mice, FPEG flavones intensely stained β-amyloid plaques. In addition, they displayed good uptake into and a rapid washout from the brain after injection in normal mice. The combination of high binding affinity for β-amyloid plaques, high brain uptake, and good clearance in mice of the FPEG-flavone derivatives may provide a series of promising in vivo amyloid imaging agents for PET.

Acknowledgments

This study was supported by the Industrial Technology Research Grant Program from the New Energy and Industrial Technology Development Organization (NEDO) of Japan, and the Program for Promotion of Fundamental Studies in Health Sciences of the National Institute of Biomedical Innovation (NIBIO).

References and notes

1. Hardy, J. A.; Higgins, G. A. *Science* **1992**, *256*, 184.
2. Selkoe, D. J. *Physiol. Rev.* **2001**, *81*, 741.
3. Selkoe, D. J. *Nat. Biotechnol.* **2000**, *18*, 823.
4. Mathis, C. A.; Wang, Y.; Klunk, W. E. *Curr. Pharm. Des.* **2004**, *10*, 1469.
5. Nordberg, A. *Lancet Neurol.* **2004**, *3*, 519.
6. Ono, M.; Wilson, A.; Nobrega, J.; Westaway, D.; Verhoeff, P.; Zhuang, Z. P.; Kung, M. P.; Kung, H. F. *Nucl. Med. Biol.* **2003**, *30*, 565.
7. Verhoeff, N. P.; Wilson, A. A.; Takeshita, S.; Trop, L.; Hussey, D.; Singh, K.; Kung, H. F.; Kung, M. P.; Houle, S. *Am. J. Geriatr. Psychiat.* **2004**, *12*, 584.
8. Mathis, C. A.; Wang, Y.; Holt, D. P.; Huang, G. F.; Debnath, M. L.; Klunk, W. E. *J. Med. Chem.* **2003**, *46*, 2740.
9. Klunk, W. E.; Engler, H.; Nordberg, A.; Wang, Y.; Blomqvist, G.; Holt, D. P.; Bergstrom, M.; Savitcheva, I.; Huang, G. F.; Estrada, S.; Ausen, B.; Debnath, M. L.; Barletta, J.; Price, J. C.; Sandell, J.; Lopresti, B. J.; Wall, A.; Koivisto, P.; Antoni, G.; Mathis, C. A.; Langstrom, B. *Ann. Neurol.* **2004**, *55*, 306.
10. Kudo, Y.; Okamura, N.; Furumoto, S.; Tashiro, M.; Furukawa, K.; Maruyama, M.; Itoh, M.; Iwata, R.; Yanai, K.; Arai, H. *J. Nucl. Med.* **2007**, *48*, 553.
11. Agdeppa, E. D.; Kepe, V.; Liu, J.; Flores-Torres, S.; Satyamurthy, N.; Petric, A.; Cole, G. M.; Small, G. W.; Huang, S. C.; Barrio, J. R. *J. Neurosci.* **2001**, *21*, RC189.
12. Shoghi-Jadid, K.; Small, G. W.; Agdeppa, E. D.; Kepe, V.; Ercoli, L. M.; Siddarth, P.; Read, S.; Satyamurthy, N.; Petric, A.; Huang, S. C.; Barrio, J. R. *Am. J. Geriatr. Psychiat.* **2002**, *10*, 24.
13. Rowe, C. C.; Ackerman, U.; Browne, W.; Mulligan, R.; Pike, K. L.; O'Keefe, G.; Tochon-Danguy, H.; Chan, G.; Berlangieri, S. U.; Jones, G.; Dickinson-Rowe, K. L.; Kung, H. P.; Zhang, W.; Kung, M. P.; Skovronsky, D.; Dyrks, T.; Holl, G.; Krause, S.; Friebe, M.; Lehman, L.; Lindemann, S.; Dinkelborg, L. M.; Masters, C. L.; Villemagne, V. L. *Lancet Neurol.* **2008**, *7*, 129.
14. Ono, M.; Yoshida, N.; Ishibashi, K.; Haratake, M.; Arano, Y.; Mori, H.; Nakayama, M. *J. Med. Chem.* **2005**, *48*, 7253.
15. Stephenson, K. A.; Chandra, R.; Zhuang, Z. P.; Hou, C.; Oya, S.; Kung, M. P.; Kung, H. F. *Bioconjugate Chem.* **2007**, *18*, 238.
16. Ono, M.; Kung, M. P.; Hou, C.; Kung, H. F. *Nucl. Med. Biol.* **2002**, *29*, 633.
17. Zhuang, Z. P.; Kung, M. P.; Wilson, A.; Lee, C. W.; Plossl, K.; Hou, C.; Holtzman, D. M.; Kung, H. F. *J. Med. Chem.* **2003**, *46*, 237.
18. Cheng, Y.; Prusoff, W. *Biochem. Pharmacol.* **1973**, *1973*, 3099.
19. Ares, J. J.; Outt, P. E.; Randall, J. L.; Murray, P. D.; Weisshaar, P. S.; O'Brien, L. M.; Erns, B. L.; Kakodkar, S. V.; Kelm, G. R.; Kershaw, W. C., et al *J. Med. Chem.* **1995**, *38*, 4937.
20. Ono, M.; Haratake, M.; Mori, H.; Nakayama, M. *Bioorg. Med. Chem.* **2007**, *15*, 6802.
21. Ono, M.; Hori, M.; Haratake, M.; Tomiyama, T.; Mori, H.; Nakayama, M. *Bioorg. Med. Chem.* **2007**, *15*, 6388.
22. Zhang, W.; Oya, S.; Kung, M. P.; Hou, C.; Maier, D. L.; Kung, H. F. *Nucl. Med. Biol.* **2005**, *32*, 799.

Please cite this article in press as: Ono, M. et al., *Bioorg. Med. Chem.* (2009), doi:10.1016/j.bmc.2009.01.025

BRAIN RESEARCH 1212 (2008) 18–24

available at www.sciencedirect.com

ScienceDirect

www.elsevier.com/locate/brainres

BRAIN RESEARCH

Research Report

PET O-15 cerebral blood flow and metabolism after acute stroke in spontaneously hypertensive rats

Takashi Temma[a], *Yuji Kuge*[a], *Kohei Sano*[a], *Junko Kamihashi*[a], *Naoyuki Obokata*[a], *Hidekazu Kawashima*[b], *Yasuhiro Magata*[c], *Hideo Saji*[a,*]

[a]*Department of Patho-Functional Bioanalysis, Graduate School of Pharmaceutical Sciences, Kyoto University, 46-29 Yoshida Shimoadachi-cho, Sakyo-ku, Kyoto 606-8501, Japan*

[b]*Department of Nuclear Medicine and Diagnostic Imaging, Graduate School of Medicine, Kyoto University, 54 Shogoin Kawahara-cho, Sakyo-ku, Kyoto 606-8507, Japan*

[c]*Laboratory of Genome Bio-Photonics, Photon Medical Research Center, Hamamatsu University School of Medicine, 1-20-1 Handayama, Higashi-ku, Hamamatsu 431-3192, Japan*

ARTICLE INFO

Article history:
Accepted 18 March 2008
Available online 29 March 2008

Keywords:
Cerebral metabolic rate for oxygen
Oxygen extraction fraction
Hypertension
Positron emission tomography
Spontaneously hypertensive rats
Stroke

ABSTRACT

Hypertension is a major stroke risk factor and is correlated with worse outcome after stroke. Thus, the effects of hypertension on cerebral hemodynamics and metabolism within an hour after stroke must be evaluated in detail. Cerebral blood flow (CBF), oxygen extraction fraction (OEF), cerebral metabolic rate for oxygen ($CMRO_2$) and cerebral metabolic rate for glucose (CMRglc) were measured 1 h after the occlusion of the right middle cerebral artery (MCA) in male spontaneously hypertensive rats (SHR) and male normotensive Wistar Kyoto rats (WKY). Physiological responses were determined by positron emission tomography (PET) using ^{15}O-H_2O and radiolabeled ^{15}O-O_2 blood (methodology previously developed in this laboratory) and by autoradiography (ARG) using ^{18}F-FDG. The right hemisphere of SHR showed lower CBF values than the left hemisphere after stroke (right: 0.17±0.07 mL/min/g; left: 0.29±0.08 mL/min/g), $CMRO_2$ (right: 2.55±0.80 mL/min/100 g; left: 4.11± 0.84 mL/min/100 g) and CMRglc (right: 52.4±16.2 mg/min/100 g; left: 65.6±10.2 mg/min/100 g). WKY rats exhibited significant decreases only in CBF and $CMRO_2$. These results suggest greater underlying physiologic disturbances in SHR. Also, the occlusion significantly reduced CBF in both hemispheres of SHR compared with WKY, suggesting a disturbance of the autoregulatory mechanism in SHR. In summary, our results indicate that hypertension intensifies metabolic disturbances after the onset of stroke, at least in the first hour. Therefore, we suggest that hypertension not only increases the incidence of stroke but also exacerbates stroke-mediated damage.

1. Introduction

Hypertension increases the incidence of stroke and degrades functional outcome following the onset of stroke. Several reports detail the comparatively poorer outcome of hypertensive patients following stroke (Leonardi-Bee et al., 2002; Sprigg et al., 2006). Hypertension is known to cause long-lasting damage to blood vessels and tissues (Amenta et al., 2003;

* *Corresponding author*. Fax: +81 75 753 4568.
E-mail address: hsaji@pharm.kyoto-u.ac.jp (H. Saji).

0006-8993/$ – see front matter © 2008 Elsevier B.V. All rights reserved.
doi:10.1016/j.brainres.2008.03.033

Fredriksson et al., 1984; Grabowski et al., 1993), altering cerebral blood flow (CBF), oxygen extraction fraction (OEF), cerebral metabolic rate for oxygen ($CMRO_2$) and cerebral metabolic rate for glucose (CMRglc) (Fujishima et al., 1995; Fujishima et al., 1984). Accordingly, it is of great importance to clarify the relationship of hypertension to cerebral hemodynamics and metabolism, and functional outcome.

It is impractical to measure such parameters in patients during the first hours following a stroke because of the demands of the therapeutic time window. Consequently, several researchers have studied the progress of cerebral hemodynamics and metabolism after the onset of stroke using spontaneously hypertensive rats (SHR), a widely employed hypertensive model (Fujishima et al., 1984; Fukuda et al., 2004; Grabowski et al., 1993; Katsuta, 1997; Okamoto and Aoki, 1963; Sadoshima et al., 1985). However, due to methodologic limitations in evaluating cerebral oxygen metabolism, only CBF and infarction have been examined (Dogan et al., 1998; Jacewicz et al., 1992). To the best of our knowledge, no report has focused on the relationship between hypertension and changes of cerebral oxygen metabolism after the onset of stroke. We recently developed a radiopharmaceutical, injectable ^{15}O-O_2 for use in positron emission tomography (PET) and established a method for estimating cerebral oxygen metabolism in small animals (Magata et al., 2003; Temma et al., 2006).

In this study, we evaluated the effects of hypertension on cerebral hemodynamics and metabolism in the first hour following the onset of stroke. Specifically, we measured CBF, OEF, $CMRO_2$ and CMRglc using injectable ^{15}O-O_2 and 2-[^{18}F]fluoro-2-deoxy-D-glucose (^{18}F-FDG) in SHR. This allowed us to measure differences in metabolic responses between SHR and normotensive rats 1 h after arterial occlusion.

2. Results

2.1. Physiological parameters

Table 1 summarizes arterial blood gas measurements before the occlusion of the MCA (pre) and after the PET experiments (post). The blood gas levels were within physiological ranges, although slight differences in several parameters were found between pre and post and between SHR and WKY.

Table 1 – Arterial blood gas values before MCA occlusion (pre) and after the PET experiments (post)

	Pre		Post	
	SHR	WKY	SHR	WKY
pH	7.33 (0.02)	7.32 (0.04)	7.29 (0.07)	7.25 (0.03)¶
pCO_2 (mm Hg)	44.8 (4.3)	46.4 (4.7)	41.1 (8.5)	48.2 (8.1)
pO_2 (mm Hg)	94.3 (13.1)	81.2 (7.1)*	101.2 (3.3)	86.8 (7.1)*
Hct (%)	54 (3.2)	48.8 (1.3)*	50.8 (2.7)¶	49.5 (2.1)
O_2Sat (%)	96.3 (1)	94.5 (1.6)*	97 (1.1)	94.7 (1.4)*
Hb (g/dl)	18.4 (1.1)	16.6 (0.4)*	17.3 (0.9)¶	16.8 (0.7)
BP (mm Hg)	129 (15.5)	105 (18.7)*	112 (18.8)¶	103 (21.7)
HR (bpm)	275 (25.4)	280 (58.4)	313 (37.9)	327 (53.2)

Statistical differences in each physiological parameter between pre and post and between SHR and WKY at the time point were determined using the Wilcoxon signed rank test; ¶$p<0.05$ vs. pre-value, and Mann–Whitney U-test; *$p<0.05$ vs. SHR, respectively. Values listed are means (s.d.).

2.2. Quantitative values

Fig. 1 shows the values and statistical analyses for CBF, OEF, $CMRO_2$ and CMRglc. SHR showed significant differences between the left and right hemispheres in CBF, $CMRO_2$ and CMRglc, while WKY showed differences in CBF, OEF and $CMRO_2$. Regarding differences between SHR and WKY, CBF and OEF values differed significantly in both the left and right hemispheres. In addition, preliminary investigations using normal SHR ($n=4$) showed CBF, OEF and $CMRO_2$ values of 0.45 ± 0.05 mL/min/g, 0.41 ± 0.02 and 4.38 ± 0.41 mL/min/100 g, respectively, in the entire brain.

2.3. Injured area following MCAO

As depicted in Fig. 2, the injured area revealed by TTC staining of each coronal slice was larger in SHR than in WKY rats as determined by two-factor repeated measures ANOVA ($F[2.112, 0.098]=21.554$, $p<0.001$).

3. Discussion

It has been suggested that hypertension affects the brain's physiologic responses after the onset of stroke. In this study, we measured parameters of cerebral hemodynamics and metabolism such as CBF, OEF, $CMRO_2$ and CMRglc 1 h after the occlusion of the MCA in SHR.

The area damaged by the occlusion was larger in SHR than in WKY rats. Thus, our experimental system is consistent with previous reports (Dogan et al., 1998; Grabowski et al., 1993). Our experiments provided the following results. First, both SHR and WKY rats showed a statistically significant decrease in CBF and $CMRO_2$ values in the right hemisphere compared with the left. Second, SHR exhibited a significant difference in CMRglc values between the hemispheres. This observation was not made in WKY rats. Third, SHR did not show significant differences in OEF between the hemispheres, unlike WKY rats. Fourth, both hemispheres of SHR showed a decrease in CBF and an increase in OEF values compared with WKY rats. Finally, in SHR, the right hemisphere exhibited an extensive (but not significant) decrease in $CMRO_2$ compared with that in WKY.

The results obtained here suggest that 1 h after the onset of MCAO, greater (injurious) metabolic changes occurred in the brains of SHR than WKY rats. This is the first report using a small animal model to evaluate the effects of hypertension on metabolic functions in the first hour following arterial occlusion. SHR exhibited significantly greater metabolic impairment 1 h after the onset of MCAO than did WKY. Thus, hypertension should be recognized as a risk factor for the onset of stroke as well as for poorer outcome after stroke. The experiments also demonstrated that the injectable ^{15}O-O_2-PET system can be an effective approach for evaluating rats' response to novel pharmaceutical agents in the setting of stroke and brain metabolism.

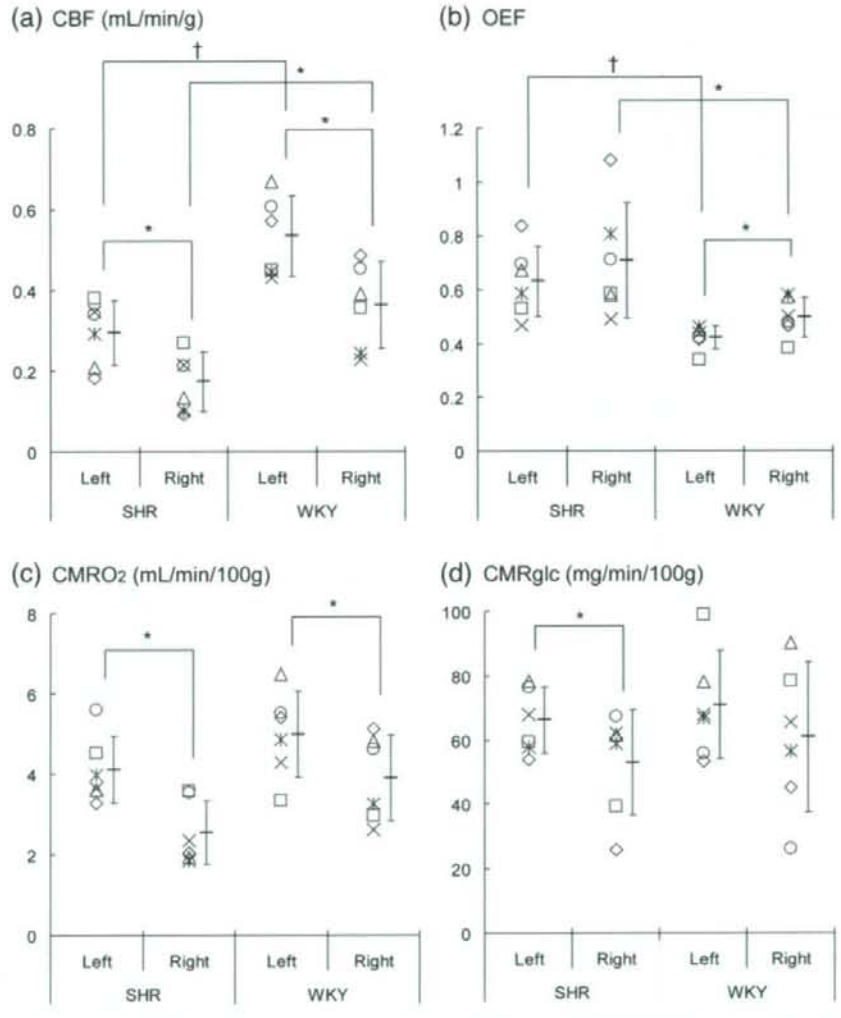

Fig. 1 – Quantitative values of (a) CBF (mL/min/g), (b) OEF, (c) $CMRO_2$ (mL/min/100 g), and (d) CMRglc (mg/min/100 g). Each of the six marks indicates the hemispheric average of four slices in an individual. Bar-shaped marks adjacent to the six individual marks show the averages of the rats and the error bars represent standard deviations. Significant differences between hemispheres and between SHR and WKY were determined using the Wilcoxon signed rank test; $^{*}p<0.05$, and the Mann–Whitney U-test; $^{*}p<0.05$, $^{\dagger}p<0.01$.

In both SHR and WKY, the right hemisphere showed significant decreases of $CMRO_2$ compared with the left hemisphere. In the left hemisphere, there was no significant difference in $CMRO_2$ values between SHR and WKY unlike the difference in CBF. These results suggest that the compensatory mechanism functioned well, as indicated by the increased OEF in the left hemisphere of SHR in comparison to the OEF values of normal SHR. In the right hemisphere, a statistically significant difference in $CMRO_2$ data was not observed for SHR and WKY, unlike CBF. However, $CMRO_2$ tended to decrease in SHR compared with WKY rats ($p=0.0547$). Hence, we speculate that the compensatory mechanism in SHR might partially function.

There was a significant difference between CMRglc values in the hemispheres of SHR. Since the PET data was analyzed in one hemisphere in view of the relatively low spatial resolution of the system (SHR-7700L) (Watanabe et al., 1997), the CMRglc values were also calculated in the same ROIs. Accordingly, two explanations for the CMRglc values in WKY rats are possible, with some caution regarding the results showing a higher value in the right hemisphere than the left in one out of six animals. First, the right hemisphere might not be damaged enough to provide a sufficient difference in comparison with the left. This possibility is unlikely because the results for $CMRO_2$ show a significant decrease in the right hemisphere compared with the left. Second, it is possible that the CMRglc

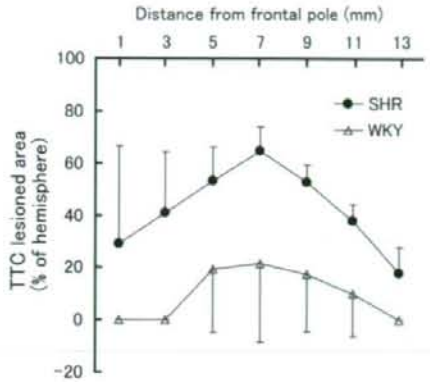

Fig. 2 – The damaged area revealed by TTC staining was evaluated 7 h after MCAO. The error bars represent standard deviations. There was a significant difference, $p<0.001$, between SHR and WKY as estimated with a two-factor repeated measures ANOVA.

value obtained in the right hemisphere of WKY reflects total tissue metabolism including anaerobic glycolysis as reported previously (Kita et al., 1995). Actually, in this study, the autoradiographic images exhibited an almost uniform accumulation of ^{18}F-FDG throughout the right hemisphere of WKY, probably because the occluding period was limited to 1 h. $CMRO_2$ and CMRglc have different meanings which are derived from accumulation mechanisms of radiopharmaceuticals to tissues or analytical methods. Accordingly, they could be used together to precisely evaluate the disturbance after stroke.

Astrocytes contribute to the consumption of glucose in the brain (Hertz, 2004; Thoren et al., 2005, 2006). Therefore, a difference in the quantity or distribution of astrocytes in the brains of SHR and WKY rats might influence the CMRglc values. It was previously reported, though, that SHR at 14 weeks of age displayed few changes in brain morphology, compared with age-matched WKY rats (Sabbatini et al., 2001). Thus, structural differences in cell distribution probably did not impact the results.

As for OEF, SHR exhibited higher values in both hemispheres. This outcome might reflect a mechanism to compensate for the decreased CBF, maintaining oxygen metabolism in brain tissues. On the other hand, WKY rats showed an increase in OEF only in the right hemisphere as in our previous report using SD rats (Temma et al., 2006). The OEF values in the right hemisphere of SHR were widely dispersed compared with WKY, indicating further disturbances in SHR (Nemoto et al., 2004; Powers, 1991). Also, there were several points with OEF values exceeding 1.0 in the right hemisphere of SHR, perhaps attributable to very low isotopic signals obtained in the two PET scans. Low signal strength might have been due to the remarkable decrease in CBF corresponding to the decreased oxygen metabolism.

Compared with WKY, SHR exhibited significantly lower CBF values in both hemispheres. The decrease in the left hemisphere seems curious, but the same result has been reported previously (Grabowski et al., 1993; Kita et al., 1995). The collateral circulation in SHR is reduced in the structurally altered vascular bed (Fredriksson et al., 1984; Grabowski et al., 1993). Hypertension is known to cause structural changes such as hypertrophy and remodeling in cerebral arteries (Amenta et al., 2003) followed by a disturbance of the autoregulatory mechanism in SHR (Fujishima et al., 1984; Yasuda et al., 2002). Thirteen to seventeen-week old SHR were used in this study because their autoregulatory mechanism is less impaired. However, the MCAO procedure might have induced a serious decrease of perfusion pressure in both hemispheres, rendering CBF unsustainable in SHR. Also, a steal-like phenomenon from vessels leading to poorly oxygenated regions might cause CBF to decrease in the left hemisphere in SHR. In addition, pCO_2 is known to affect CBF, but the difference between SHR and WKY was not striking enough to induce the significant decrease in CBF in SHR (Heinert et al., 1998).

SHR are widely used in studies of hypertension because the condition arises naturally in the rats with aging, similar in character to essential-hypertension in humans. Although the causes of essential-hypertension in humans, or the factors resulting in hypertension in SHR have not been fully elucidated, SHR is now regarded as the best animal model for hypertension (Fujishima et al., 1984; Fukuda et al., 2004; Grabowski et al., 1993; Katsuta, 1997; Okamoto and Aoki, 1963; Sadoshima et al., 1985). It is known that the blood pressure of SHR reaches a plateau after around 10 weeks of age (Fukuda et al., 2004; Okamoto and Aoki, 1963), and long-standing hypertension can cause increased contractility of arteries and impaired autoregulation of CBF (Fujishima et al., 1984; Katsuta, 1997; Sadoshima et al., 1985). For those reasons, 13 to 17-week old SHR were used in this study.

Blood gases were analyzed several times during the PET experiments. In the experiments, pO_2, Hct, O_2Sat and Hb were significantly different between SHR and WKY rats before the operation, as reported previously (Fukuda et al., 2004). Such differences might reflect the compensatory process for delivery of oxygen in the setting of high systemic pressure persistent in SHR. It is also notable that the pH of WKY rats and Hct, Hb and BP of SHR decreased after the experiments in comparison with the pre-MCAO values. Thus, injection of 2 mL of ^{15}O-O_2 or continuous blood sampling during two PET scans may have had adverse effects.

4. Conclusions

In this paper, we estimated CBF, OEF, $CMRO_2$ and CMRglc 1 h after the onset of MCAO in SHR. SHR exhibited greater disturbances of metabolic parameters compared with WKY rats, indicating that hypertension probably contributes to degraded metabolic functions and poorer prognosis after the onset of stroke.

5. Experimental procedures

5.1. Animals

Male SHR (13–17 week old, 276–330 g) and male Wistar Kyoto rats (WKY, 14–17 week old, 314–388 g) were supplied by Japan SLC Co. (Hamamatsu, Japan) and were housed under a 12 h

light/12 h dark cycle and given free access to food and water. The animal experiments in this study were conducted in accordance with institutional guidelines and approved by the Kyoto University Animal Care Committee.

5.2. *Preparation of labeled compounds*

The production of ^{15}O-H_2O and injection of ^{15}O-oxygenated blood (injectable ^{15}O-O_2) were conducted as reported previously (Magata et al., 2003; Temma et al., 2006). In brief, ^{15}O-H_2O was synthesized by the reduction of ^{15}O-O_2 with H_2 gas (catalyzed by Pd black at 140 °C) and trapped in a saline solution. Injectable ^{15}O-O_2 was prepared by the following procedure: first, part of an infusion line kit (Terumo Corporation, Tokyo, Japan) and an artificial lung 18 cm in length (Senko Medical Instruments Mfg Co. Ltd., Tokyo, Japan) were connected using silicon tubing to make a closed system. Then, 18 to 20 mL of blood collected from several rats was added to the system and circulated (100 mL/min) by a peristaltic pump (EYELA roller pump RP-1000, Tokyo Rikakikai Co. Ltd., Tokyo, Japan). Finally, ^{15}O-O_2 gas (3000–5450 MBq/min/500 mL) was introduced into the artificial lung for 15 min to prepare injectable ^{15}O-O_2 (43 to 130 MBq/mL). ^{18}F-FDG was synthesized by the nucleophilic substitution method with an ^{18}F-FDG-synthesizing instrument, the F-100 (Sumitomo Heavy Industries, Co. Ltd., Tokyo, Japan) (Hamacher et al., 1986; Kitano et al., 2001).

5.3. *Preparation of animals*

The rats were divided into two groups, one for the PET experiment and the other for the autoradiographic (ARG) experiment. Fig. 3 shows an outline of the experiments. In the PET experiment, six SHR and six WKY rats were subjected to middle cerebral artery occlusion (MCAO). CBF, OEF and $CMRO_2$ were evaluated using ^{15}O-H_2O and injectable ^{15}O-O_2. In the ARG experiment, six SHR and six WKY rats were subjected to MCAO and CMRglc was evaluated using ^{18}F-FDG. The rats fasted for 6 h prior to the operation and then were anesthetized with chloral hydrate (i.p. 400 mg/kg). The left femoral artery in each rat was catheterized using a PE 20 catheter (i.d. 0.5 mm, o.d. 0.8 mm) for blood sampling during the experiments. Then, the right middle cerebral artery (MCA) was occluded intraluminally using a nylon 4-0 monofilament (Kuge et al., 1995; Longa et al., 1989; Minematsu et al., 1992). After the MCAO procedure, the rats were administered 100 IU of heparin (i.v.). Rectal temperature was maintained at approximately 37 °C with the aid of heating pads. Blood pressure was measured during the experiments. Blood gases were measured several times during the course of the experiments using 100 μL of blood and a portable blood gas analyzer (i-STAT®300F, FUSO Pharmaceutical Industries, Ltd., Osaka, Japan).

5.4. *PET experiments*

The PET experiments were performed according to methods reported previously (Magata et al., 2003; Temma et al., 2006). The animal was placed supine in a stereotaxic apparatus and restrained. After the acquisition of a blank scan for 180 min, the apparatus was placed in a PET scanner (SHR-7700L, Hamamatsu Photonics, Hamamatsu, Japan) designed for scanning small animals. For a high-resolution animal study the system was modified with compact PS-PMT detectors, achieving a spatial resolution of 2.7 mm in the plane and 3.3 mm in the axial direction with the full width at half maximum (Watanabe et al., 1997). The position was standardized with the aid of a laser beam and the desired cranial position in the scanner was oriented. A transmission scan was performed for 30 min for attenuation correction. Forty minutes after the initiation of MCAO, a dynamic PET scan (12×10-second frames) was started with the simultaneous initiation of ^{15}O-H_2O administration (i.v., 148 to 222 MBq over a 30-second period) to obtain CBF values. Arterial blood sampling was performed as 10 μL×18 times in the scan. After the radioactivity of ^{15}O-H_2O had decayed, that is, 60 min after the initiation of MCAO, a second PET scan (12×10-second frames) was started with the simultaneous initiation of injectable ^{15}O-O_2 administration

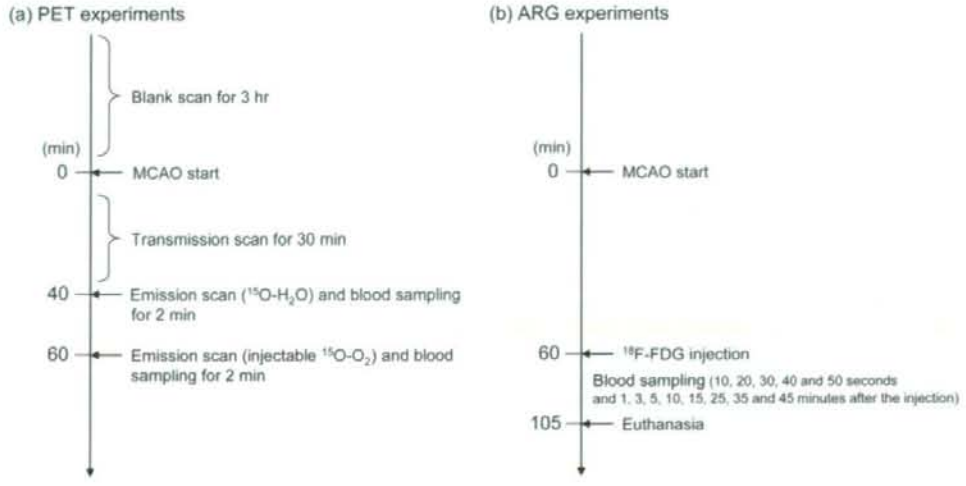

Fig. 3 – Outline of the experiments. (a) PET experiments and (b) ARG experiments.

(i.v., 74 to 148 MBq over a 60-second period) in order to measure OEF values. Arterial blood sampling was performed continuously throughout the PET scans (50–100 μL×13 times) to measure radioactivity in blood and plasma. The radioactivity of each sample was measured with an NaI well-type scintillation counter (Packard AutoGamma 500, Packard Instruments, Meriden, CT, U.S.A.) calibrated using a ^{22}Na standard radioactive source. Saline was injected into the animal to maintain the blood volume during experiments. The animal was allowed to recover from anesthesia after the PET scans and euthanized 7 h after MCAO. The brain was removed and 2 mm thick coronal sections were prepared with a McIlwain Tissue Chopper (Mickle Laboratory Engineering Co. Ltd., Surrey, United Kingdom) and used for triphenyltetrazolium chloride (TTC) staining. Areas not stained red with TTC represented regions of severe tissue injury. The damaged areas were expressed as follows: (((TTC-stained area in the left (normal) hemisphere)−(TTC-stained area in the right (injured) hemisphere))/(TTC-stained area in the left (normal) hemisphere))×100.

5.5. *ARG experiments*

^{18}F-FDG (74 MBq/kg) was administered intravenously 1 h after the initiation of MCAO. Arterial blood sampling (50–100 μL) was performed at 10, 20, 30, 40 and 50 s and 1, 3, 5, 10, 15, 25, 35 and 45 min after the injection. Plasma concentrations of F-18 radioactivity and glucose were determined using the scintillation counter and a glucose measurement kit (Glucose CII-Test, Wako Pure Chemical Industries Ltd., Osaka, Japan), respectively. Immediately after the last blood sampling, the rats were euthanized and their brains were rapidly removed, frozen, and cut into 20-μm thick sections with a cryostat microtome. The sections were thaw-mounted on precleaned silane-coated slides and placed on a Fuji Imaging Plate (BAS-SR, Fuji Photo Film, Tokyo, Japan) for 2 h. The autoradiograms were analyzed using a computerized imaging analysis system (Bio Imaging Analyzer BAS2500 and Image Gauge, Fuji Photo Film, Tokyo, Japan).

5.6. *Data analysis*

PET images were reconstructed according to a standard filtered back-projection procedure using a Hamming filter. The rat brain was visualized in four consecutive coronal slices. Then, two regions of interest (ROIs, 60 to 110 mm^3), from the right and left hemispheres, were visually chosen according to the magnetic resonance images obtained previously in another study using 1.5 T MRI. Activity in ROIs was calibrated using a cross calibration factor obtained in another phantom study with a 10 cm diameter hollow phantom.

The CBF value in each ROI was calculated by numerically solving Eq. (1) as reported previously (Temma et al., 2004). Eq. (1) is $R(t) = f \cdot A_W(t) * e^{-\left(\frac{f}{p}+\lambda\right)t}$, where the asterisk denotes the convolution integral, the tissue concentration of O-15 radioactivity is shown by ($R(t)$), CBF is (f), the arterial concentration of ^{15}O-water radioactivity is ($A_W(t)$), the partition coefficient of water between the brain and blood is (p=0.8) and the physical decay constant of O-15 is (λ).

The OEF value was calculated using the same equation (Eq. (2)) as that applied to the bolus inhalation of ^{15}O-O$_2$ gas (Mintun et al., 1984; Shidahara et al., 2002) which can also be used with injectable ^{15}O-O$_2$ as shown previously (Magata et al., 2003; Temma et al., 2006). Eq. (2) is $R(t) = \mathrm{OEF} \cdot f \cdot A_O(t) * e^{-\left(\frac{f}{p}+\lambda\right)t} + f \cdot A_W(t) * e^{-\left(\frac{f}{p}+\lambda\right)t} + V_B \cdot R \cdot (1 - V_V' \cdot \mathrm{OEF}) \cdot A_O(t)$, where the arterial concentration of ^{15}O-O$_2$ radioactivity is ($A_O(t)$), cerebral blood volume is (V_B=0.04 mL/g), the hematocrit ratio between central and peripheral regions is (R=0.85) and the effective venous ratio in the brain is (V_V'= 0.835).

The $CMRO_2$ value was calculated using Eq. (3). Eq. (3) is $CMRO_2 = \frac{(1.39 \times Hb \times \%Sat)}{100} \times OEF \times CBF$ in which Hb is gram hemoglobin/mL blood and %Sat is percent saturation of O_2 (Shidahara et al., 2002).

The CMRglc value was calculated by the autoradiographic method (Sokoloff et al., 1977), adopting values of 0.19 min^{-1}, 0.25 min^{-1} and 0.052 min^{-1} for k_1^*, k_2^* and k_3^*, respectively, and a value of 0.46 for the lumped constant.

5.7. *Statistics*

The significance of differences for values between the left and right hemispheres was assayed with the Wilcoxon signed rank test. The significance of differences in values between SHR and WKY was estimated with the Mann–Whitney U-test unless noted otherwise. A p value<0.05 was considered statistically significant.

Acknowledgments

This study was supported by Grants-in-Aid for Scientific Research and by the 21st Century Center of Excellence Programs at Kyoto University "Knowledge Information Infrastructure for Genome Science" and at Hamamatsu University School of Medicine "Medical Photonics" from the Ministry of Education, Culture, Sports, Science and Technology, Japan. Part of this study was supported by the Mitsubishi Pharma Research Foundation.

REFERENCES

Amenta, F., et al., 2003. Arterial hypertension and brain damage — evidence from animal models (review). Clin. Exp. Hypertens. 25, 359–380.

Dogan, A., et al., 1998. Intraluminal suture occlusion of the middle cerebral artery in spontaneously hypertensive rats. Neurol. Res. 20, 265–270.

Fredriksson, K., et al., 1984. The hemodynamic effect of bilateral carotid artery ligation and the morphometry of the main communicating circuit in normotensive and spontaneously hypertensive rats. Acta Physiol. Scand. 121, 241–247.

Fujishima, M., et al., 1995. Cerebral blood flow and brain function in hypertension. Hypertens. Res. 18, 111–117.

Fujishima, M., et al., 1984. Autoregulation of cerebral blood flow in young and aged spontaneously hypertensive rats (SHR). Gerontology 30, 30–36.

Fukuda, S., et al., 2004. Age-related changes in blood pressure, hematological values, concentrations of serum biochemical constituents and weights of organs in the SHR/Izm, SHRSP/Izm and WKY/Izm. Exp. Anim. 53, 67–72.

Grabowski, M., et al., 1993. Brain capillary density and cerebral blood flow after occlusion of the middle cerebral artery in

normotensive Wistar-Kyoto rats and spontaneously hypertensive rats. J. Hypertens. 11, 1363–1368.
Hamacher, K., et al., 1986. Efficient stereospecific synthesis of no-carrier-added 2-[18F]-fluoro-2-deoxy-D-glucose using aminopolyether supported nucleophilic substitution. J. Nucl. Med. 27, 235–238.
Heinert, G., et al., 1998. Hypercapnic cerebral blood flow in spontaneously hypertensive rats. J. Hypertens. 16, 1491–1498.
Hertz, L., 2004. Intercellular metabolic compartmentation in the brain: past, present and future. Neurochem. Int. 45, 285–296.
Jacewicz, M., et al., 1992. The CBF threshold and dynamics for focal cerebral infarction in spontaneously hypertensive rats. J. Cereb. Blood Flow Metab. 12, 359–370.
Katsuta, T., 1997. Decreased local cerebral blood flow in young and aged spontaneously hypertensive rats. Fukuoka Igaku Zasshi 88, 65–74.
Kita, H., et al., 1995. Cerebral blood flow and glucose metabolism of the ischemic rim in spontaneously hypertensive stroke-prone rats with occlusion of the middle cerebral artery J. Cereb. Blood Flow Metab. 15, 235–241.
Kitano, H., et al., 2001. Performance assessment of O-18 water purifier. Ann. Nucl. Med. 15, 75–78.
Kuge, Y., et al., 1995. Nylon monofilament for intraluminal middle cerebral artery occlusion in rats. Stroke 26, 1655–1657 discussion 1658.
Leonardi-Bee, J., et al., 2002. Blood pressure and clinical outcomes in the International Stroke Trial. Stroke 33, 1315–1320.
Longa, E.Z., et al., 1989. Reversible middle cerebral artery occlusion without craniectomy in rats. Stroke 20, 84–91.
Magata, Y., et al., 2003. Development of injectable O-15 oxygen and estimation of rat OEF. J. Cereb. Blood Flow Metab. 23, 671–676.
Minematsu, K., et al., 1992. Diffusion-weighted magnetic resonance imaging: rapid and quantitative detection of focal brain ischemia. Neurology 42, 235–240.
Mintun, M.A., et al., 1984. Brain oxygen utilization measured with O-15 radiotracers and positron emission tomography. J. Nucl. Med. 25, 177–187.
Nemoto, E.M., et al., 2004. Identification of hemodynamic compromise by cerebrovascular reserve and oxygen extraction fraction in occlusive vascular disease. J. Cereb. Blood Flow Metab. 24, 1081–1089.
Okamoto, K., Aoki, K., 1963. Development of a strain of spontaneously hypertensive rats. Jpn. Circ. J. 27, 282–293.
Powers, W.J., 1991. Cerebral hemodynamics in ischemic cerebrovascular disease. Ann. Neurol. 29, 231–240.
Sabbatini, M., et al., 2001. Hypertensive brain damage: comparative evaluation of protective effect of treatment with dihydropyridine derivatives in spontaneously hypertensive rats. Mech. Ageing Dev. 122, 2085–2105.
Sadoshima, S., et al., 1985. Upper limit of cerebral autoregulation during development of hypertension in spontaneously hypertensive rats — effect of sympathetic denervation Stroke 16, 477–481.
Shidahara, M., et al., 2002. Evaluation of a commercial PET tomograph-based system for the quantitative assessment of rCBF, rOEF and rCMRO2 by using sequential administration of 15O-labeled compounds Ann. Nucl. Med. 16, 317–327.
Sokoloff, L., et al., 1977. The [14C]deoxyglucose method for the measurement of local cerebral glucose utilization: theory, procedure, and normal values in the conscious and anes thetized albino rat. J. Neurochem. 28, 897–916.
Sprigg, N., et al., 2006. Relationship between outcome and baseline blood pressure and other haemodynamic measures in acute ischaemic stroke: data from the TAIST trial. J. Hypertens. 24, 1413–1417.
Temma, T., et al., 2006. Estimation of oxygen metabolism in a rat model of permanent ischemia using positron emission tomography with injectable15O-O2. J. Cereb. Blood Flow Metab. 26, 1577–1583.
Temma, T., et al., 2004. Availability of N-isopropyl-p-[125I] iodoamphetamine (IMP) as a practical cerebral blood flow (CBF) indicator in rats. Nucl. Med. Biol. 31, 811–814.
Thoren, A.E., et al., 2005. Astrocytic function assessed from 1-14C-acetate metabolism after temporary focal cerebral ischemia in rats. J. Cereb. Blood Flow Metab. 25, 440–450.
Thoren, A.E., et al., 2006. The metabolism of C-glucose by neurons and astrocytes in brain subregions following focal cerebral ischemia in rats. J. Neurochem. 97, 968–978.
Watanabe, M., et al., 1997. A high resolution animal PET scanner using compact PS-PMT detectors. IEEE Trans. Nucl. Sci. 44, 1277–1282.
Yasuda, T., et al., 2002. Persistent hypertension does not alter the cerebral blood flow and glucose utilization in young-adult Dahl salt-sensitive rats. J. Neurol. Sci. 197, 19–26.

Available online at www.sciencedirect.com
ScienceDirect
Nuclear Medicine and Biology 35 (2008) 213–218
NUCLEAR MEDICINE — AND — BIOLOGY
www.elsevier.com/locate/nucmedbio

Evaluation of radioiodinated (2*S*,α*S*)-2-(α-(2-iodophenoxy)benzyl) morpholine as a radioligand for imaging of norepinephrine transporter in the heart

Yasushi Kiyono[a,c,*], Taku Sugita[b], Masashi Ueda[c], Hidekazu Kawashima[d], Naoki Kanegawa[b], Yuji Kuge[b], Yasuhisa Fujibayashi[a], Hideo Saji[b]

[a]*Biomedical Imaging Research Center, University of Fukui, Fukui 910-1193, Japan*
[b]*Department of Pathofunctional Bioanalysis, Graduate School of Pharmaceutical Sciences, Kyoto University, Kyoto 606-8501, Japan*
[c]*Radioisotopes Research Laboratory, Kyoto University Hospital, Faculty of Medicine, Kyoto University, Kyoto 606-8507, Japan*
[d]*Department of Nuclear Medicine and Diagnostic Imaging, Graduate School of Medicine, Kyoto University, Kyoto 606-8507, Japan*

Received 5 September 2007; received in revised form 23 November 2007; accepted 23 November 2007

Abstract

Introduction: The norepinephrine transporter (NET) is located presynaptically on noradrenergic nerve terminals and plays a critical role in the regulation of the synaptic norepinephrine (NE) concentration via the reuptake of NE. Changes in NET have been recently reported in several cardiac failures. Therefore, a NET-specific radioligand is useful for in vivo assessment of changes in NET density in various cardiac disorders. Recently, we developed a radioiodinated reboxetine analogue, (2*S*,α*S*)-2-(α-(2-iodophenoxy)benzyl)morpholine ((*S*,*S*)-IPBM), for NET imaging. In the current study, we assessed the applicability of radioiodinated (*S*,*S*)-IPBM to NET imaging in the heart.

Methods: The NET affinity and selectivity were measured from the ability to displace specific [^{3}H]nisoxetine and (*S*,*S*)-[^{125}I]IPBM binding to rat heart membrane, respectively. To evaluate the distribution of (*S*,*S*)-[^{125}I]IPBM in vivo, biodistribution experiment was performed in rats. With the use of several monoamine transporter binding agents, pharmacological blocking experiments were performed in rats.

Results: In vitro binding assays showed that the affinity of (*S*,*S*)-IPBM to NET was similar to those of the well-known NET-specific binding agents, nisoxetine and desipramine. Furthermore, (*S*,*S*)-[^{125}I]IPBM binding was inhibited by nisoxetine and desipramine, but not by dopamine or serotonin transporter binding agents. These data indicated that (*S*,*S*)-IPBM had high affinity and selectivity for NET in vitro. Biodistribution studies in rats showed rapid and high uptake of (*S*,*S*)-[^{125}I]IPBM by the heart and rapid clearance from the blood. The heart-to-blood ratio was 31.9 at 180 min after the injection. The administration of nisoxetine and desipramine decreased (*S*,*S*)-[^{125}I]IPBM accumulation in the heart, but injection of fluoxetine and GBR12909 had little influence.

Conclusions: Radioiodinated (*S*,*S*)-IPBM is a potential radioligand for NET imaging in the heart.

Keywords: Norepinephrine transporter; Sympathetic nervous function; SPECT; Radioiodination; (*S*,*S*)-IPBM; Heart

1. Introduction

The norepinephrine transporter (NET) is located presynaptically on noradrenergic nerve terminals and plays a critical role in the regulation of synaptic concentrations of norepinephrine (NE) in the noradrenergic nervous system by the reuptake of NE [1]. In the heart, NET exists in sympathetic nerve terminals. Changes in NET have been reported in several cardiac failures [2–7]. Furthermore, this NET has been recently noted as a therapeutic target [8–10]. Two pieces of information are necessary for estimating this NET function precisely. One is the transport activity of NET, and the other is the density of NET in sympathetic nerve terminals. To evaluate the first information, [^{123}I]meta-iodobenzylguanidine (MIBG) and [^{11}C]hydroxyephedrine, NET substrates, have been widely used for the imaging of cardiac

* Corresponding author. Biomedical Imaging Research Center, University of Fukui, 23-3, Matsuokashimoaizuki, Eiheiji, Yoshida, Fukui 910-1193, Japan. Tel.: +81 776 61 8420; fax: +81 776 61 8170.
E-mail address: ykiyono@u-fukui.ac.jp (Y. Kiyono).

0969-8051/$ – see front matter © 2008 Elsevier Inc. All rights reserved.
doi:10.1016/j.nucmedbio.2007.11.006

sympathetic nervous function in various cardiovascular diseases [11–13]. These radiolabeled NET substrates are taken up by sympathetic nerve terminals, stored into vesicles and secreted to sympathetic clefts, and therefore images of these NET substrates reflect the overall function of nervous terminals. The information on NET density could be also important for predicting the effect of NET targeting therapy and/or understanding the condition of cardiac diseases.

A radioligand bound to NET could be potentially useful for studying the role of the NE reuptake system in these diseased states and for predicting the therapeutic effect of NET targeting drugs. Therefore, the development of a radioligand to bind NET has been of great interest.

We recently synthesized radioiodinated (*R*)-*N*-methyl-3-(2-iodophenoxy)-3-phenylpropamine ((*R*)-MIPP) as a NET binding agent. However, this radioligand had a slight affinity to serotonin transporter (SERT) in vivo in the brain and heart [14,15]. More recently, we developed radioiodinated (2*S*,α*S*)-2-(α-(2-iodophenoxy)benzyl)morpholine ((*S*,*S*)-IPBM), which was more selective for NET compared with (*R*)-MIPP in the brain [15,16].

In this study, the applicability of radioiodinated (*S*,*S*)-IPBM to NET imaging in the heart was evaluated by investigating the affinity and selectivity for NET in the heart and biodistribution including pharmacological blocking experiments and comparison with MIBG.

2. Materials and methods

2.1. Materials

[^{125}I]MIBG was supplied by Daiichi Radioisotope Laboratories (Tokyo, Japan). Sodium [^{125}I]iodide (643.8 GBq/mg) and [^{3}H]nisoxetine (2.96 TBq/mmol) were purchased from New England Nuclear (Boston, MA, USA). All chemicals used in this study were of reagent grade.

2.2. Radiosynthesis

(*S*,*S*)-[^{125}I]IPBM was obtained by a halogen exchange reaction with sodium [^{125}I]iodine according to the methods of Kanegawa et al. [15]. Briefly, (*S*,*S*)-BPBM was added to a mixture of sodium [^{125}I]-iodine, ammonium sulfate and copper (II) sulfate pentahydrate in a vial. The reaction mixture was heated for 45 min at 130°C. After cooling, the reaction mixture was extracted with methanol and filtered with a 0.22-μm filter. The filtered extract was applied to a reverse-phase high-performance liquid chromatography (HPLC) column (Cosmosil 5C_{18}-AR-300 Packed Column, 250×10 mm id, Nacalai Tesque, Kyoto, Japan) and eluted with 20 mM phosphate buffer (pH 2.5)/acetonitrile=72:28 at a flow rate of 2.0 ml/min [R_t=42 min for (*S*,*S*)-BPBM, 58 min for (*S*,*S*)-IPBM]. An adequate amount of ethanol was added to the separated (*S*,*S*)-[^{125}I]-IPBM fraction.

The radiochemical purity of the labeled compound was determined by analytical HPLC. Analytical HPLC was performed on a 150×4.6 mm id, Cosmosil AR-300 column (Nacalai Tesque, Kyoto, Japan) eluted with 20 mM phosphate buffer (pH 2.5)/acetonitrile=72:28 at a flow rate of 1.0 ml/min (R_t=15.0 min).

2.3. In vitro binding assay

The preparation of synaptosomal membranes from rat hearts was carried out according to a previously reported method with some modifications [17]. Briefly, the heart ventricles were homogenized in 20 volumes of ice-cold 250 mM sucrose buffer (5 mM Tris/HCl; 1 mM $MgCl_2$; 250 mM sucrose) with a 30-s burst, using a Polytron PT10-35 set at speed 6. The homogenate was centrifuged at 750×*g* for 10 min. The pellet was discarded and the supernatant recentrifuged at 20,000×*g* for 20 min. The resulting pellet was resuspended in 10 volumes of ice-cold 50 mM Tris-HCl buffer (50 mM Tris/HCl, 5 mM KCl, 120 mM NaCl, pH 7.4) and recentrifuged to give a pellet that was resuspended in 5 vol of the Tris-HCl buffer. The suspension was stored at −80°C until use. The protein concentration was measured by the Lowry method [18].

[^{3}H]Nisoxetine and (*S*,*S*)-[^{125}I]IPBM competition assays were performed according to the methods of Raisman et al. [17] with some modification. The assays were carried out by incubating 400 μl of the heart preparation (0.25 mg/ml) with [^{3}H]nisoxetine (2.5 nM) and various concentrations of competitors in 150 μl of 50 mM Tris-HCl buffer (50 mM Tris/HCl, 5 mM KCl, 120 mM NaCl, pH 7.4). Incubation was performed for 30 min at 25°C. At the end of the incubation, the mixture was poured into 5 ml of ice-cold Tris-HCl buffer, rapidly filtered through Whatman GF/B fiber filters and washed with 3×5 ml of buffer. For [^{3}H] nisoxetine, the radioactivity bound to the filter was measured with a liquid scintillation counter (2500-TR, Packard). For (*S*,*S*)-[^{125}I]IPBM, the radioactivity bound to the filters was measured with a NaI well scintilation counter (Cobra II Auto-Gamma, Packard). All incubations were performed in triplicate. Nonspecific binding was determined in the presence of 1 mM nisoxetine. IC_{50} values were determined from displacement curves of the percent inhibition of [^{3}H] nisoxetine and (*S*,*S*)-[^{125}I]IPBM binding vs. the inhibitor concentration using the GraphPad Prism software (GraphPad Software, San Diego, CA, USA).

(*S*,*S*)-[^{125}I]IPBM saturation assays were performed according to our previous method for brain with some modification [16]. Four hundred microliters of membrane (0.25 mg/ml) was mixed with 50 μl of (*S*,*S*)-[^{125}I]IPBM (0.01–3.0 nM). Incubation was performed for 60 min at 25°C. At the end of the incubation, the mixture was poured into 5 ml of ice-cold Tris-HCl buffer, rapidly filtered through Whatman GF/B fiber filters and washed with 3×5 ml of buffer, and the radioactivity was measured with a NaI well scintilation counter. Nonspecific binding was determined in the presence of 1 mM nisoxetine. K_D value was determined with GraphPad Prism.

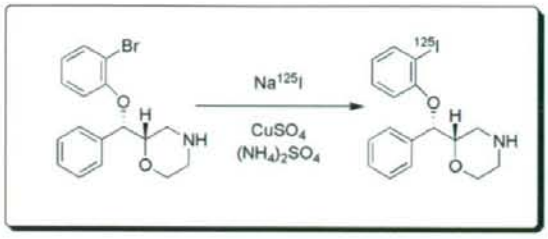

Fig. 1. Radiosynthesis of (*S,S*)-[^{125}I]IPBM.

2.4. Animals

Animal studies were conducted in accordance with our institutional guidelines, and the experimental procedures were approved by the Kyoto University Animal Care Committee.

2.5. Biodistribution experiments

Biodistribution studies were performed by intravenous administration of (*S,S*)-[^{125}I]IPBM (74 kBq) to 10-week-old male Sprague-Dawley rats. At appropriate time points after the administration, rats were sacrificed by decapitation under light ether anesthesia. Samples of blood and the organ of interest were excised and weighed, and the radioactivity was measured with an auto-well gamma counter (Aloka ARC2000, Tokyo, Japan).

2.6. Pharmacological blocking experiments

For pharmacological blocking studies, Sprague-Dawley rats were intravenously injected with (*S,S*)-[^{125}I]IPBM and various inhibitors. Nisoxetine (1 mg/kg) and desipramine (1 mg/kg) were used as NET binding agents. Fluoxetine (1 mg/kg) was used as a SERT binding agent. GBR12909 (1 mg/kg) was used for the dopamine transporter (DAT) binding agent. These agents were simultaneously injected with (*S,S*)-[^{125}I]IPBM. The animals were sacrificed 60 min after receiving (*R*)-[^{125}I]IPBM.

2.7. MIBG biodistribution experiments

To assess the potential of cardiac sympathetic nervous imaging agent, the comparison with MIBG was performed. [^{125}I]MIBG (74 kBq) was intravenously injected to 10-week-old male Sprague-Dawley rats. At 15, 60 and 180 min postinjection, rats were sacrificed by decapitation under light ether anesthesia. Samples of blood and the organ of heart and liver were excised and weighed, and the radioactivity was measured with an auto-well gamma counter.

Table 1
Inhibition of [^{3}H]nisoxetine binding to rat heart membrane

Compound	IC_{50} (nM)
(*RR/SS*)-IPBM	22.0±7.22
(*SS*)-IPBM	10.9±6.82
(*RR*)-IPBM	67.6±13.7
Nisoxetine	9.00±0.84
Desipramine	5.96±0.83
Reboxetine	16.0±5.59

Each value represents the mean±S.D. of three independent experiments.

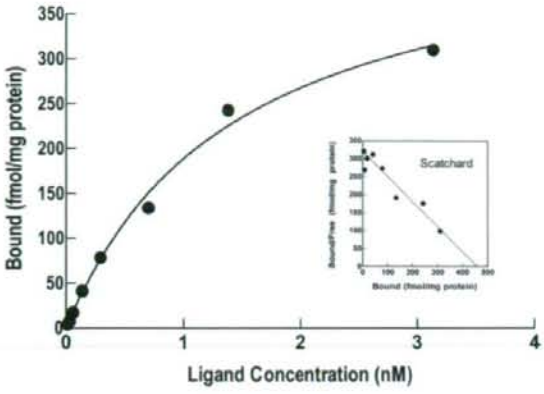

Fig. 2. Scatchard analysis of (*S,S*)-IPBM binding to rat heart membranes. The binding affinity was 1.63±0.22 nM.

2.8. Statistical analyses

Data are presented as mean values with the S.D. Comparisons were performed with the unpaired alternate Welch *t*-test. $P<.05$ was considered statistically significant.

3. Results

3.1. Radiosynthesis

The synthesis of no-carrier-added (*S,S*)-[^{125}I]IPBM was carried out by bromine-radioiodine exchange reaction (Fig. 1). The radiochemical yield of (*S,S*)-[^{125}I]IPBM was about 65% and the radiochemical purity was greater than 99%.

3.2. In vitro binding assay

In vitro binding assays showed that the affinity of (*S,S*)-IPBM (IC_{50}=10.9 nM) to NET was similar to those of the well-known NET inhibitors, nisoxetine and desipramine (IC_{50}=9.0 and 6.0 nM; Table 1). The specific binding of (*S,S*)-IPBM was saturable with a high affinity, and Scatchard transformation of the binding data gave a linear plot

Table 2
Inhibition of (*S,S*)-[^{125}I]IPBM binding to rat heart membrane

Compound	IC_{50} (nM)
Nisoxetine	2.28±0.87
Desipramine	6.86±2.71
Fluoxetine	1165±204
GBR12909	>10,000

Each value represents the mean±S.D. of three independent experiments.

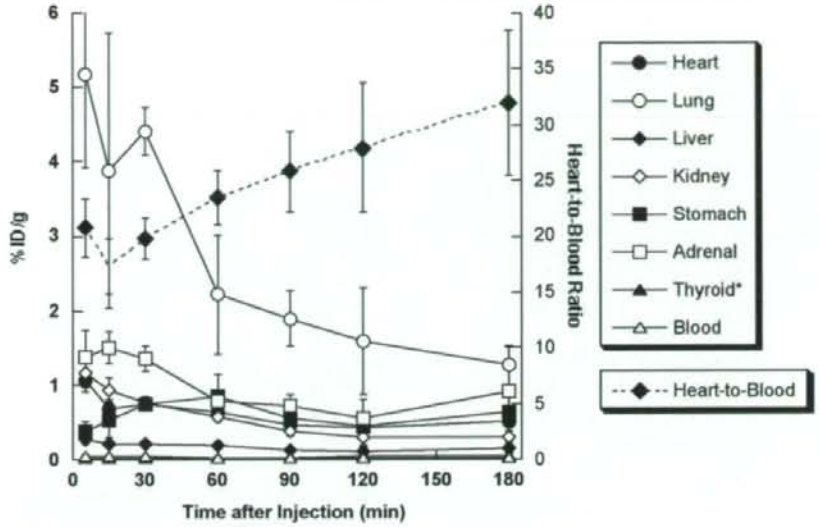

Fig. 3. Biodistribution of (*S,S*)-[^{125}I]IPBM in rats. Biodistribution of radioactivity is expressed as percentage of injected ^{125}I dose/gram of organ. Each point represents the mean±S.D. Only the data of thyroid represent the percentage of injected ^{125}I/organ.

indicating one-site binding (Fig. 2). The mean values gave a K_D value of 1.63±0.22 nM. Furthermore, (*S,S*)-[^{125}I]IPBM binding was inhibited by NET inhibitors, nisoxetine and desipramine (IC_{50}=2.28 and 6.86 nM; Table 2). However, (*S,S*)-[^{125}I]IPBM binding was only slightly inhibited by fluoxetine (IC_{50}=1165 nM; Table 2) and hardly inhibited at all by GBR12909 (IC_{50} >10,000 nM; Table 2). These data indicate that (*S,S*)-IPBM has a high affinity and selectivity for NET in vitro.

3.3. Biodistribution experiments

Fig. 3 shows the results of biodistribution studies in rats. The results showed rapid and high uptake of (*S,S*)-[^{125}I] IPBM by the heart and rapid clearance from the blood. The heart-to-blood ratio was increased with time, and the maximum value was 31.9 at 180 min after the injection. A high accumulation of (*S,S*)-[^{125}I]IPBM was observed in the lungs and adrenals, in which NET was abundant. The radioactivity in the liver was low. The level of radioactivity in the thyroid was also low, which indicated high stability of (*S,S*)-[^{125}I]IPBM to in vivo deiodination.

3.4. Pharmacological blocking experiments

The effects of various monoamine transporter inhibitors on the heart uptake of (*S,S*)-[^{125}I]IPBM were studied. Injection of nisoxetine and desipramine, NET binding agents, decreased the accumulation of (*S,S*)-[^{125}I]IPBM in the heart to about 40% at 60 min after injection (Fig. 4). However, the administration of fluoxetine and GBR12909 did not have significant effects on the accumulation of (*S,S*)-[^{125}I]IPBM in the heart.

3.5. Comparison of the biodistribution of (S,S)-[^{125}I]IPBM with [^{125}I]MIBG

The comparison of the biodistribution of (*S,S*)-[^{125}I] IPBM with [^{125}I]MIBG in 15-, 60- and 180-min phases is summarized in Table 3. The heart uptake of [^{125}I]MIBG was higher than that of (*S,S*)-[^{125}I]IPBM in each time point.

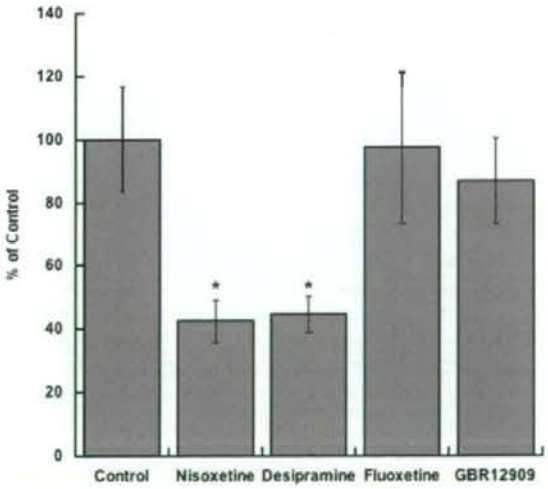

Fig. 4. Effect of various inhibitors on the cardiac uptake of (*S,S*)-[^{125}I]IPBM in rats. (*S,S*)-[^{125}I]IPBM was simultaneously injected with NET inhibitors, nisoxetine (1 mg/kg) and desipramine (1 mg/kg); a SERT inhibitor, fluoxetine (1 mg/kg); and a DAT inhibitor, GBR12909 (1 mg/kg). Rats were sacrificed at 60 min after injection. *P<.001 vs. control.

Table 3
Biodistribution of (*S,S*)-[^{125}I]IPBM compared with [^{125}I]MIBG

		15 min	60 min	180 min
Heart	IPBM	0.66±0.13	0.64±0.07	0.50±0.13
	MIBG	2.78±0.22	1.95±0.85	2.11±0.17
Liver	IPBM	0.20±0.03	0.20±0.02	0.15±0.03
	MIBG	0.75±0.14	0.29±0.11	0.18±0.03
Blood	IPBM	0.039±0.007	0.027±0.003	0.016±0.003
	MIBG	0.18±0.04	0.13±0.06	0.12±0.02
Heart/blood ratio	IPBM	17.3±2.45	23.5±2.38	31.9±6.44
	MIBG	16.4±3.78	15.7±5.79	18.3±1.51

Biodistribution of radioactivity is expressed as percentage of injected ^{125}I dose/gram of organ (mean±S.D.).

Regarding liver uptake, the uptake of [^{125}I]MIBG in 15 and 60 min was higher than that of (*S,S*)-[^{125}I]IPBM. However, there was no significant difference in 180 min. The heart-to-blood ratio of (*S,S*)-[^{125}I]IPBM was higher than that of [^{125}I] MIBG in each time point.

4. Discussion

The basic requirements for an effective radiolabeled NET binding agent for molecular imaging of cardiac NET density include a high binding affinity and selectivity for the NET protein, and high heart uptake.

With respect to the affinity and selectivity, in vitro binding studies using the heart synaptosomal membranes showed that (*S,S*)-IPBM had a high affinity as well as nisoxetine, desipramine and reboxetine, the typical NET binding agents (Table 1). Furthermore, nisoxetine and desipramine inhibited the (*S,S*)-[^{125}I]IPBM binding, but fluoxetine slightly inhibited that binding and GBR12909 did not (Table 2). These results show that (*S,S*)-[^{125}I]IPBM has high affinity and selectivity for myocardial NET.

In biodistribution studies, (*S,S*)-[^{125}I]IPBM showed a high uptake followed by a rapid clearance in the heart. This distribution pattern in the heart was consistent with that of other radioligands for NET imaging [14,19,20]. Compared with (*R*)-[^{125}I]MIPP, the initial uptake of (*S,S*)-[^{125}I]IPBM was slightly lower [(*S,S*)-IPBM: 1.06 %ID/g, (*R*)-MIPP: 1.36 %ID/g, at 5 min postinjection]. However, at 180 min postinjection, accumulation of (*S,S*)-IPBM was higher than that of (*R*)-MIPP [(*S,S*)-IPBM: 0.50 %ID/g, (*R*)-MIPP: 0.27 %ID/g] [14]. These data suggest that the clearance of (*S,S*)-IPBM was slower than that of (*R*)-MIPP because (*S,S*)-IPBM bound to NET more selectively than (*R*)-MIPP. Furthermore, the heart-to-blood ratio of (*S,S*)-[^{125}I]IPBM was higher than that of (*R*)-[^{125}I]MIPP [(*S,S*)-IPBM: 23.5 (60 min) and 31.9 (180 min), (*R*)-MIPP: 13.0 (60 min) and 7.5 (180 min)] [14]. This is due to the higher accumulation of (*S,S*)-IPBM in the heart and faster clearance of (*S,S*)-IPBM from the blood. The administration of nisoxetine and desipramine, NET-specific binding agents, decreased (*S,S*)-[^{125}I]IPBM accumulation in the heart, but injection of fluoxetine and GBR12909 had little influence. These results indicated that (*S,S*)-[^{125}I]IPBM selectively accumulated for NET in the heart. Gathering these data, we considered radioiodinated (*S,S*)-IPBM to be a more suitable agent for cardiac NET imaging compared with (*R*)-MIPP. In the pharmacological blocking studies, however, about 40% of the radioactivity remained in the heart. Although the cause of this binding is not clear, it is most likely due to high nonspecific binding due to high lipophilicity. This high residual uptake may result in a high background uptake, especially in the denervated heart, and limit the clinical utility of this agent. More studies are required of this high residual uptake.

The uptake in the lung was higher than that in the heart at each point. This may be due to the binding to NET in the lung [21], other binding sites and/or amine metabolic enzymes, such as monoamine oxidase, in the lung [22–24]. It is predicted that a SPECT image will show less accumulation in the lung than the value in biodistribution studies because of the existence of a large amount of air in the lung of a living body. Further imaging studies with (*S,S*)-[^{123}I]IPBM may be required.

To compare with MIBG, the heart uptake of (*S,S*)-[^{125}I] IPBM was lower than that of [^{125}I]MIBG (Table 3). However, the washout rate (uptake of 15 min/uptake of 180 min) of (*S, S*)-[^{125}I]IPBM in the heart was similar to that of [^{125}I]MIBG (IPBM=1.32±0.43 and MIBG=1.32±0.15). Regarding liver uptake, the liver uptake of (*S,S*)-[^{125}I]IPBM in 15 and 60 min was lower than that of [^{125}I]MIBG, although both uptakes were similar in 180 min. In other words, the uptake of (*S,S*)-[^{125}I]IPBM in the liver was kept in low level. However, the uptake of [^{125}I]MIBG was high level in the early phase, then [^{125}I]MIBG was gradually decreased from the liver. Since high hepatic accumulation is a problem in [^{123}I]MIBG diagnosis [25], this low accumulation of (*S,S*)-IPBM in the liver may be an advantage over MIBG. The heart-to-blood ratio (imaging index of heart) of (*S,S*)-[^{125}I]IPBM was significantly higher than that of [^{125}I]MIBG. This may also be an advantage of (*S,S*)-[^{125}I]IPBM.

In conclusion, (*S,S*)-IPBM showed a high affinity and selectivity for NET in vitro and in vivo in the heart. Although further investigation is required, these results indicate that radioiodinated (*S,S*)-IPBM is a potential radioligand for NET imaging in the heart.

Acknowledgments

We would like to thank Daiichi Radioisotope Laboratories Ltd., Tokyo, Japan, for providing [^{125}I]MIBG. This study was supported in part by Grants-in-Aid for Scientific Research on Priority Areas (Research on Pathomechanisms of Brain Disorders) from the Ministry of Education, Culture, Sports, Science and Technology of Japan (18023023).

References

[1] Mandela P, Ordway GA. The norepinephrine transporter and its regulation. J Neurochem 2006;97:310–33.

[2] Backs J, Haunstetter A, Gerber SH, Metz J, Borst MM, Strasser RH, et al. The neuronal norepinephrine transporter in experimental heart failure: evidence for a posttranscriptional downregulation. J Mol Cell Cardiol 2001;33:461–72.

[3] Bohm M, La Rosee K, Schwinger RH, Erdmann E. Evidence for reduction of norepinephrine uptake sites in the failing human heart. J Am Coll Cardiol 1995;25:146–53.

[4] Fukumitsu N, Suzuki M, Fukuda T, Kiyono Y, Kajiyama S, Saji H. Reduced ^{125}I-meta-iodobenzylguanidine uptake and norepinephrine transporter density in the hearts of mice with MPTP-induced parkinsonism. Nucl Med Biol 2006;33:37–42.

[5] Kiyono Y, Iida Y, Kawashima H, Ogawa M, Tamaki N, Nishimura H, et al. Norepinephrine transporter density as a causative factor in alterations in MIBG myocardial uptake in NIDDM model rats. Eur J Nucl Med Mol Imaging 2002;29:999–1005.

[6] Shannon JR, Flattem NL, Jordan J, Jacob G, Black BK, Biaggioni I, et al. Orthostatic intolerance and tachycardia associated with norepinephrine-transporter deficiency. N Engl J Med 2000;342:541–9.

[7] Ungerer M, Chlistalla A, Richardt G. Upregulation of cardiac uptake 1 carrier in ischemic and nonischemic rat heart. Circ Res 1996;78: 1037–43.

[8] Keller NR, Diedrich A, Appalsamy M, Tuntrakool S, Lonce S, Finney C, et al. Norepinephrine transporter-deficient mice exhibit excessive tachycardia and elevated blood pressure with wakefulness and activity. Circulation 2004;110:1191–6.

[9] Munch G, Rosport K, Bultmann A, Baumgartner C, Li Z, Laacke L, et al. Cardiac overexpression of the norepinephrine transporter uptake-1 results in marked improvement of heart failure. Circ Res 2005;97:928–36.

[10] Schroeder C, Birkenfeld AL, Mayer AF, Tank J, Diedrich A, Luft FC, et al. Norepinephrine transporter inhibition prevents tilt-induced presyncope. J Am Coll Cardiol 2006;48:516–22.

[11] Carrio I. Cardiac neurotransmission imaging. J Nucl Med 2001;42: 1062–76.

[12] Langer O, Halldin C. PET and SPET tracers for mapping the cardiac nervous system. Eur J Nucl Med Mol Imaging 2002;29:416–34.

[13] Yamashina S, Yamazaki J. Neuronal imaging using SPECT. Eur J Nucl Med Mol Imaging 2007;34:939–50.

[14] Kiyono Y, Kanegawa N, Kawashima H, Fujiwara H, Iida Y, Nishimura H, et al. A new norepinephrine transporter imaging agent for cardiac sympathetic nervous function imaging: radioiodinated (*R*)-*N*-methyl-3-(2-iodophenoxy)-3-phenylpropanamine. Nucl Med Biol 2003;30: 697–706.

[15] Kiyono Y, Kanegawa N, Kawashima H, Kitamura Y, Iida Y, Saji H. Evaluation of radioiodinated (*R*)-*N*-methyl-3-(2-iodophenoxy)-3-phenylpropanamine as a ligand for brain norepinephrine transporter imaging. Nucl Med Biol 2004;31:147–53.

[16] Kanegawa N, Kiyono Y, Kimura H, Sugita T, Kajiyama S, Kawashima H, et al. Synthesis and evaluation of radioiodinated (*S,S*)-2-(alpha-(2-iodophenoxy)benzyl)morpholine for imaging brain norepinephrine transporter. Eur J Nucl Med Mol Imaging 2006;33:639–47.

[17] Raisman R, Sette M, Pimoule C, Briley M, Langer SZ. High-affinity [^{3}H]desipramine binding in the peripheral and central nervous system: a specific site associated with the neuronal uptake of noradrenaline. Eur J Pharmacol 1982;78:345–51.

[18] Lowry OH, Rosebrough NJ, Farr AL, Randall RJ. Protein measurements with the Folin phenol reagent. J Biol Chem 1951; 193:265–75.

[19] Haka MS, Kilbourn MR. Synthesis and regional mouse brain distribution of [^{11}C]nisoxetine, a norepinephrine uptake inhibitor. Int J Rad Appl Instrum B 1989;16:771–4.

[20] Nakamura H, Edo K, Hishinuma T, Takahashi T, Ido T, Mizugaki M. Synthesis of ^{11}C-labeled imipramine and its biodistribution in mice: a potential tracer for positron emission tomography. Chem Pharm Bull (Tokyo) 1989;37:3376–9.

[21] Tseng YT, Padbury JF. Expression of a pulmonary endothelial norepinephrine transporter. J Neural Transm 1998;105:1187–91.

[22] Fowler JS, Gallagher BM, MacGregor RR, Wolf AP. Carbon-11 labeled aliphatic amines in lung uptake and metabolism studies: potential for dynamic measurements in vivo. J Pharmacol Exp Ther 1976;198:133–45.

[23] Moretti JL, Zini R, Morin D, Joulin Y, Desplanches G, Caillat-Vigneron N, et al. Interactions of phenylalkylamines with human lung membrane and microsome preparation. Nucl Med Commun 1987;8: 115–20.

[24] Touya JJ, Rahimian J, Grubbs DE, Corbus HF, Bennett LR. A noninvasive procedure for in vivo assay of a lung amine endothelial receptor. J Nucl Med 1985;26:1302–7.

[25] Gill JS, Hunter GJ, Gane G, Camm AJ. Heterogeneity of the human myocardial sympathetic innervation: in vivo demonstration by iodine 123-labeled meta-iodobenzylguanidine scintigraphy. Am Heart J 1993;126:390–8.

BRAIN RESEARCH 1199 (2008) 46–52

available at www.sciencedirect.com

ScienceDirect

www.elsevier.com/locate/brainres

BRAIN RESEARCH

Research Report

5-Iodo-A-85380, a specific ligand for α4β2 nicotinic acetylcholine receptors, prevents glutamate neurotoxicity in rat cortical cultured neurons

Masashi Ueda[a,b], *Yasuhiko Iida*[c], *Youji Kitamura*[d], *Hidekazu Kawashima*[e], *Mikako Ogawa*[f], *Yasuhiro Magata*[f], *Hideo Saji*[b,*]

[a]Radioisotopes Research Laboratory, Kyoto University Hospital, Faculty of Medicine, Kyoto University, Kyoto 606-8507, Japan
[b]Department of Patho-Functional Bioanalysis, Graduate School of Pharmaceutical Sciences, Kyoto University, Kyoto 606-8501, Japan
[c]Bioimaging Information Analysis, Graduate School of Medicine, Gunma University, Maebashi, Gunma 371-8512, Japan
[d]Graduate School of Medicine and Dentistry and Pharmaceutical Sciences, Okayama University, Okayama 700-8530, Japan
[e]Department of Nuclear Medicine and Diagnostic Imaging, Graduate School of Medicine, Kyoto University, Kyoto 606-8507, Japan
[f]Laboratory of Genome-Bio Photonics, PhotonMedical Research Center, Hamamatsu University School of Medicine, Hamamatsu, Shizuoka 431-3192, Japan

ARTICLE INFO

Article history:
Accepted 15 October 2007
Available online 26 January 2008

Keywords:
Nicotinic acetylcholine receptor
α4β2 subtype
5-iodo-A-85380 (5IA)
Neuroprotection
Glutamate toxicity
Extracellular calcium ion

ABSTRACT

5-iodo-3-(2(S)-azetidinylmethoxy)pyridine (5-iodo-A-85380, 5IA) has very high affinity and selectivity to nicotinic acetylcholine receptor (nAChR) α4β2 subtype, and a relative safe profile. To assess whether 5IA has neuroprotective properties, we examined the effect of 5IA on glutamate (Glu)-induced neurotoxicity using primary cultures of rat cortical neurons. A 10-min exposure of cultures to Glu followed by 2-h incubation with drug-free medium caused a marked loss of viability, as determined by trypan blue exclusion method. Glu-induced neurotoxicity was prevented by 5IA both in a time- and concentration-dependent manner. 5IA-induced neuroprotection required pretreatment of 5IA prior to Glu exposure with an optimal concentration of 10 nM and an optimal pretreatment time of 2 h. Treatment after Glu exposure could not rescue the cultured cells. The neuroprotective effect of 5IA was antagonized by mecamylamine, a nAChR antagonist, but not by scopolamine, a muscarinic acetylcholine receptor antagonist. Dihydro-β-erythroidine, an α4β2 nAChR antagonist, completely inhibited 5IA-induced neuroprotection, whereas α-bungarotoxin, an α7 nAChR antagonist, had no effect. Furthermore, 5IA did not show neuroprotective effects in the absence of extracellular Ca^{2+}. These results suggest that the neuroprotective effects of 5IA are produced by activation of α4β2 nAChRs followed by the influx of extracellular Ca^{2+}. In conclusion, 5IA is possibly not only useful for the treatment and prevention of glutamate neurotoxicity, but also as an available tool for elucidating the mechanism of neuroprotection associated with α4β2 nAChRs.

* *Corresponding author.* Department of Patho-Functional Bioanalysis, Graduate School of Pharmaceutical Sciences, Kyoto University, 46-29 Yoshida Shimoadachi-cho, Sakyo-ku, Kyoto 606-8501, Japan. Fax: +81 75 753 4568.
E-mail address: hsaji@pharm.kyoto-u.ac.jp (H. Saji).

Abbreviations: nAChR, nicotinic acetylcholine receptor; 5IA, 5-iodo-3-(2(S)-azetidinylmethoxy)pyridine; Glu, glutamate; MEC, mecamylamine; SCOP, scopolamine; DHβE, dihydro-β-erythroidine; α-BGT, α-bungarotoxin

0006-8993/$ – see front matter © 2008 Elsevier B.V. All rights reserved.
doi:10.1016/j.brainres.2007.10.107

1. Introduction

Nicotinic acetylcholine receptors (nAChRs) are a family of ligand-gated ion channels that regulate neurotransmission in the central and peripheral nervous systems. These receptors are of great interest because they have been implicated in various brain functions, such as cognition, memory and learning (Gotti et al., 1997; Paterson and Nordberg, 2000). In addition, changes in the density of nAChRs have been reported in various neurodegenerative disorders including Alzheimer's disease (Burghaus et al., 2000; O'Brien et al., 2007; Shimohama et al., 1986) and Parkinson's disease (Burghaus et al., 2003; Fujita et al., 2006; Oishi et al., 2007).

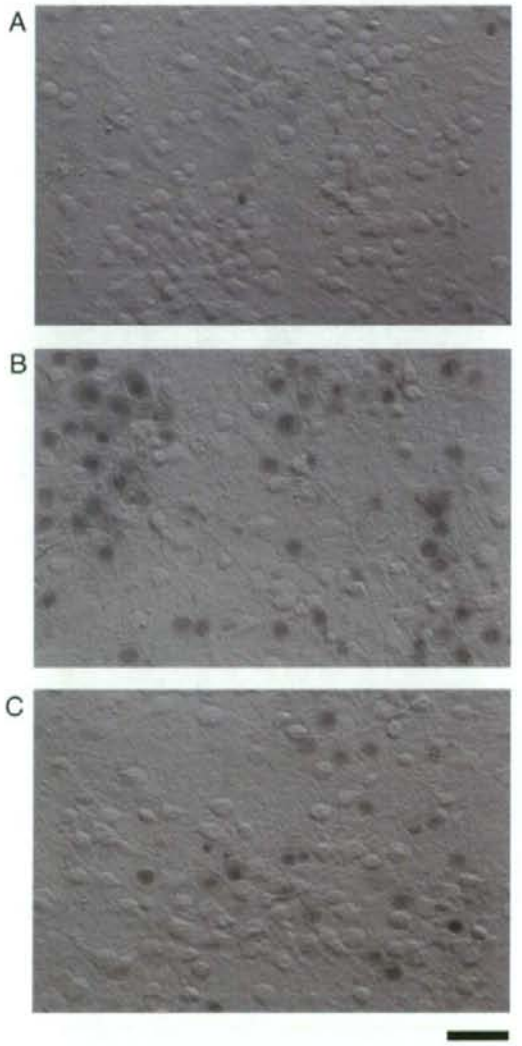

Fig. 1 – Hoffman modulation photomicrographs showing protective effects of 5IA on Glu-induced neurotoxicity. (A) indicates non-treated cells (sham). (B) shows cells treated with 1 mM of Glu for 10 min and further incubated with Glu-free EMEM for 2 h. (C) shows cells exposed to 10 nM of 5IA for 2 h before and during Glu exposure. Calibration bar = 50 μm.

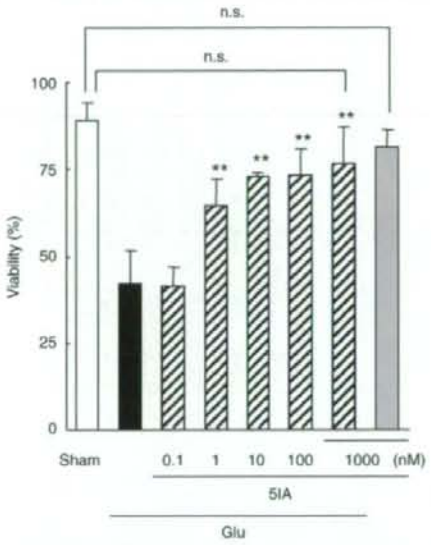

Fig. 2 – Concentration dependency of protective effects of 5IA on acute Glu neurotoxicity. Cultures were treated with 5IA (0.1–1000 nM) for 2 h before and 10 min during Glu exposure, and then incubated with drug-free EMEM for 2 h. $^{**}P<0.01$, compared with Glu alone. n.s.; not significant. Data represent the means ± s.d. of five independent observations.

Neuronal nicotinic receptors are found as pentameric assemblies that can be formed from combinations of at least 11 different receptor subunits (α2–α10 and β2–β4). Although various subtypes are expressed in the mammalian brain, two subtypes of nAChRs, α4β2 and α7, are predominant. Both subtypes have been reported to be involved in the neuroprotective effect against glutamate (Glu)-induced excitatory toxicity (Belluardo et al., 2000). The neuroprotective effects of α7 nAChRs were mediated by the activation of phosphatidylinositol 3-kinase, phosphorylation of Akt and upregulation of the anti-apoptotic protein Bcl-2 (Kihara et al., 2004; Shimohama and Kihara, 2001). On the other hand, the neuroprotective mechanisms of α4β2 nAChRs are still unknown in detail. Since neurotoxicity, mediated by Glu, is thought to play a role in progressive neurodegenerative diseases, such as Alzheimer's disease (Arias et al., 1998; Meldrum and Garthwaite, 1990), α4β2 and α7 nAChR agonists possibly delay the progression of such diseases.

Recently, 5-iodo-3-(2(S)-azetidinylmethoxy)pyridine (5-iodo-A-85380, 5IA), a derivative of A-85380 iodinated at the 5-position of the pyridine ring, was synthesized (Saji et al., 2002). The affinity of 5IA to α4β2 nAChRs was reported to be as high as that of (±)-epibatidine but low for α3β4 nAChRs, responsible for cardiovascular side effects caused by nAChR agonists (Mukhin et al., 2000). 5IA has more selectivity to α4β2 nAChRs than A-85380, the parent compound of 5IA, and in fact, studies have shown a relatively good safety profile for 5IA (Ueda et al., 2004; Vaupel et al., 2003). Thus, it is possible that 5IA will be more useful for the treatment and prevention of neurodegenerative diseases

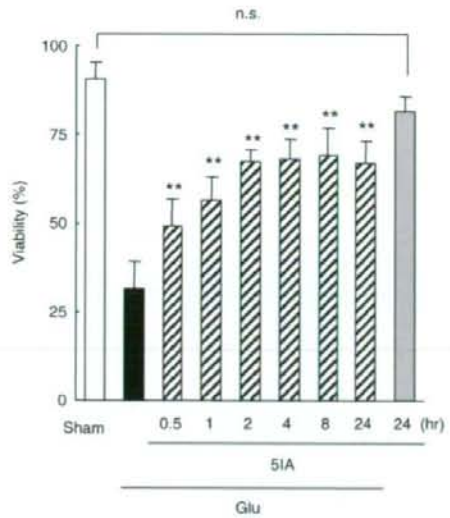

Fig. 3 – Time dependency of protective effects of 5IA on acute Glu neurotoxicity. Cultures were treated with 5IA (10 nM) for 0.5–24 h before and 10 min during Glu exposure, and then incubated with drug-free EMEM for 2 h. **P<0.01, compared with Glu alone. n.s.; not significant. Data represent the means ± s.d. of five independent observations.

than other nAChR agonists, such as nicotine. Furthermore, since 5IA has extremely high affinity and selectivity to α4β2 nAChRs, it is suitable to clarify the mechanisms of neuroprotection associated with α4β2 nAChRs.

Therefore, we assessed whether 5IA had neuroprotective properties against Glu-induced neurotoxicity using rat cortical cultures. We also elucidated the nAChR subtype and potential mechanism involved in 5IA-induced neuroprotection.

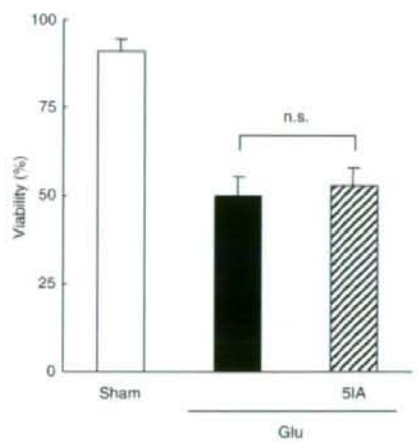

Fig. 4 – Protective effect of 5IA applied after Glu exposure. Cultures were incubated with Glu for 10 min followed by 2-h incubation in EMEM containing 10 nM of 5IA. n.s.; not significant. Data represent the means ± s.d. of five independent observations.

2. Results

2.1. *Protective effect of 5IA on glutamate-induced neurotoxicity*

We examined the effect of 5IA on Glu-induced acute neurotoxicity. Fig. 1 shows the typical protective effect of 5IA. Exposure of the cortical cultures to 1 mM of Glu for 10 min markedly increased

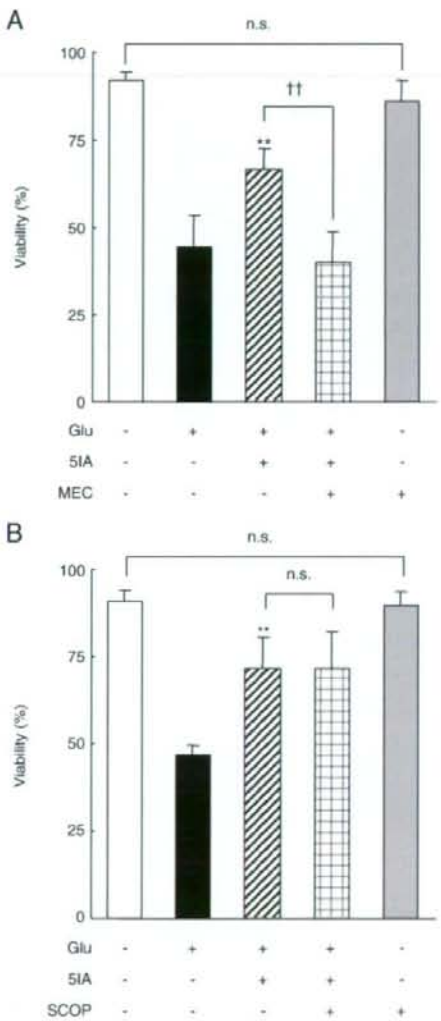

Fig. 5 – Effects of a nicotinic receptor antagonist, mecamylamine (MEC) (A) and a muscarinic receptor antagonist, scopolamine (SCOP) (B) on 5IA-induced neuroprotection against Glu toxicity. Cultures were treated with 5IA and each antagonist (1 μM) for 2 h before and 10 min during Glu exposure, and then incubated with drug-free EMEM for 2 h. **P<0.01, compared with Glu alone. ††P<0.01, compared with 5IA + Glu. n.s.; not significant. Data represent the means ± s.d. of five independent observations.

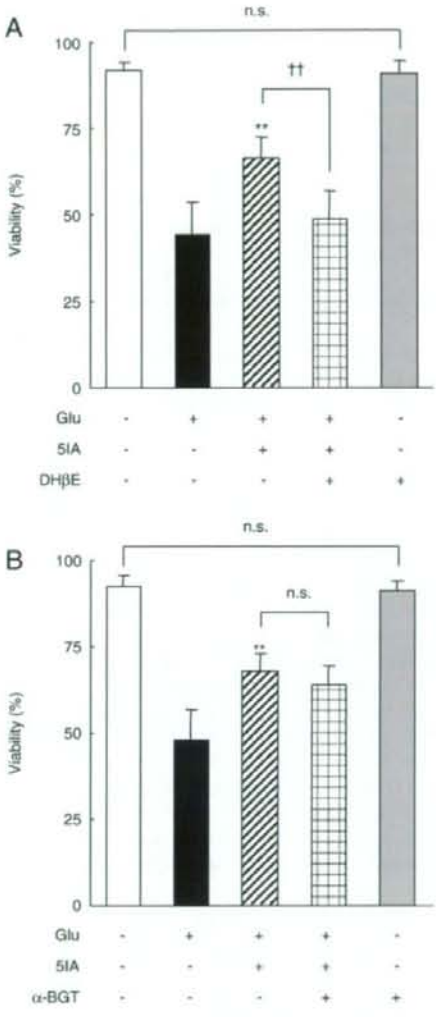

Fig. 6 – Effects of a nAChR α4β2 subtype antagonist, dihydro-β-erythroidine (DHβE) (A) and a nAChR α7 subtype antagonist, α-bungarotoxin (α-BGT) (B) on 5IA-induced neuroprotection against Glu toxicity. Cultures were treated with 5IA and each antagonist (1 μM of DHβE and 1 nM of α-BGT) for 2 h before and 10 min during Glu exposure, and then incubated with drug-free EMEM for 2 h. **P<0.01, compared with Glu alone. ††P<0.01, compared with 5IA + Glu. n.s.; not significant. Data represent the means ± s.d. of five independent observations.

the number of trypan blue-stained cells, i.e., non-viable cells (Fig. 1B). When 5IA was applied, the number of non-viable cells was markedly reduced (Fig. 1C).

Donnelly-Roberts et al. reported that the neuroprotection elicited by ABT-418 and nicotine were time dependent, with an optimal pretreatment time of 2 h (Donnelly-Roberts et al., 1996). Thus, we examined the concentration dependency of the neuroprotective effect of 5IA applied for 2 h prior to Glu exposure. One-tenth nM of 5IA produced no protection against Glu toxicity; however, 1 nM or more of 5IA increased the cell viability significantly. The protective effect reached a plateau at 10 nM (73 ± 1%) (Fig. 2).

Next, the time dependency was investigated. When we applied 10 nM of 5IA for 0.5–24 h prior to Glu exposure, 5IA showed significant protective effects at all pretreatment time points. The protective effect increased dependent on the duration of pretreatment and reached a plateau at 2 h (viability was 67 ± 4%) (Fig. 3).

We also examined the protective effect of 5IA treated after glutamate exposure. When cultures were exposed to Glu for 10 min and subsequently incubated in EMEM containing 10 nM of 5IA for 2 h, no protective effect against Glu toxicity was observed (Glu alone: 50 ± 5%, 5IA: 53 ± 5%) (Fig. 4).

2.2. *Effects of cholinergic antagonists on 5IA-induced neuroprotection*

We examined which subtype of acetylcholine receptor was involved in the neuroprotective effect of 5IA. As shown in Fig. 5, mecamylamine (MEC), a nAChR antagonist, inhibited the neuroprotective effect of 5IA (5IA: 67 ± 6%, 5IA + MEC: 40 ± 9%) and cell viability decreased to the same level as Glu alone (44 ± 10%) (Fig. 5A). On the other hand, scopolamine (SCOP), a muscarinic receptor antagonist, did not affect 5IA-induced neuroprotection at all (5IA: 71 ± 9%, 5IA + SCOP: 72 ± 11%) (Fig. 5B).

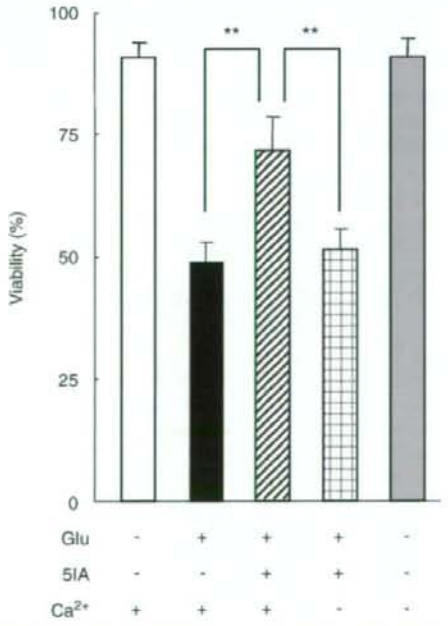

Fig. 7 – Effects of extracellular calcium ions on 5IA-induced neuroprotection against Glu toxicity. Cultures were treated with 5IA in EMEM (including Ca^{2+}) or S-MEM (excluding Ca^{2+}) for 2 h before Glu exposure. 10-min Glu exposure and following 2-h drug-free incubation were performed in EMEM. **P<0.01. Data represent the means ± s.d. of five independent observations.